Technical help for ISM investigators

IAS report T 97-01

Stéphane Erard

July 17, 1998

Institut d'Astrophysique Spatiale
Université Paris-Sud, bâtiment 121, F-91405, Orsay. France.
tel: (33) (1) 69 85 86 39 fax: (33) (1) 69 85 86 75

e-mail: erard@ias.fr

ISM is an imaging spectrometer covering the spectral range from 0.76 µm to 3.16 µm. The instrument flew on board the soviet Phobos-2 spacecraft launched on July 21st, 1988, and remained in Martian orbit from January 29th to March 27th, 1989. The data set consists in several image cubes of the surfaces of Mars and Phobos made of many pixels. Each pixel corresponds to a spectrum acquired by two arrays of cooled PbS detectors, the spectral dispersion being obtained by using a grating whose first two orders are exploited (respectively in the long and short wavelength ranges). Although the spectral resolution ($\lambda/\Delta\lambda = 60$) is comparable to that of previous ground-based observations, the angular resolution (12'x12') and the signal-to-noise ratio (up to 1500) are much better than those of any other spectral measurement on Mars, and are unchallenged so far. The experiment also provided the first spectra and the first resolved observations of Phobos in the near-infrared domain.

Three models of the instrument were built. The one that flew on Phobos-2 was called MV1 (Modèle de Vol numéro 1). MV2 was launched on Phobos-1 that was lost during its voyage to Mars, and hasn't returned any data. The spare model MV3 was later modified by CESR to fly on the ARAT airplane, a common facility to CNES and IGN, to evaluate the scientific interest of terrestrial observations in this spectral range. MV1 spent 57 days in Martian orbit and returned ≈27 Mbytes of data. First results were published in a special issue of Nature, together with a brief abstract of the mission (Sagdeev and Zakharov 1989); a complete publication list related to ISM observations is included in the data base (file PUBLISISM.ASC and .PS).

This document is released as a part of the CNES data base for ISM. It describes the instrument, explains the calibration process, and provides all useful information for future processing of the data. The data base contains all the observations made by MV1 at several

processing levels, as well as calibration files and routines, documentation, and secondary products. The original technical documentation of the instrument is not included, but is archived on printed form by CNES (in French). CNES also maintains navigation data of the Phobos mission, that may be consulted on line.

The instrument was developed by IAS (Université Paris-Sud) and DESPA (Observatoire de Paris) and was supported by CNES (French space agency). The project manager was Alain Soufflot, the Principal Investigator was Jean-Pierre Bibring, both from IAS; the lead scientist at DESPA was Michel Combes. Other French and foreign groups were early associated to data processing and interpretation, in particular Vassili Moroz's group at IKI (Moscow), Jim Head's group at Brown University (Providence), Angioletta Coradini's group at IAS (Rome), Gabriele Arnold's group at DLR (Berlin), Philippe Masson and Christophe Sotin in Orsay. The final calibration of the data presented here is the result of this common effort. For my part, I'd like to thank Jean-Pierre Bibring, Yves Langevin, Brigitte Gondet and Alain Soufflot who worked on both the data and the instrument at IAS, Jan Rosenqvist, John Mustard and Scott Murchie, whose involvement was critical in establishing this final product, Dima Titov, Laurel Kirkland and Peter Lampen, who tested preliminary versions of this archive, and all the individuals who worked on the data.

Stéphane Erard, July 1997.

The present file contain some PS figures with low-quality PICT previews that can be plotted on a screen. Beware that in some situations the previews can be printed instead of the original PS figures.

Glossary

Several words are reserved for a special use in this document.

- “Pixel” corresponds to the projection of the IFOV on the surface.
- “Order” is reserved to the light reflected on the grating.
- “Range” refers to the two separate optical paths of the instrument, long and short wavelengths, used to measure the light scattered in the first and second grating orders.
- “Array” designates the two detection devices used in the two ranges of the instrument. Each array is a set of 64 detectors in two staggered rows (odd and even).
- “Detector” refers to each of the 128 individual detectors associated to a wavelength.
- “Channel” designates each of the 128 electronic/logical paths corresponding to the detectors.
- “Row” designates a half array, or a sub-set of 32 detectors.

- The set of coefficients converting the data from digital numbers to physical units is referred to as the “transfer function” and is designed by the letter α.
- “Relative uncertainty” corresponds to the fluctuations of intensity ratio in a given channel when looking at a stable light source. It depends only on the signal-to-noise of the observations, which is typically dominated by the analogic noise in the instrument.
- “Channel-to-channel uncertainty” corresponds to the error on the intensity ratio between two neighboring channels in a given spectrum. This is essentially a systematic error related to the shape of the transfer function and removal of additive contributions.
- “Absolute uncertainty” corresponds to the error on the reflectance measured in a given channel. It depends mainly on the level of the transfer function and on the stability of the light sources used. This systematic error is typically ≈15% for spectral observations.

Optical characteristics

During an observation session, the instrument acquires a spectrum on many zones (pixels) about 10 arc minutes in angular dimension. Each spectrum is a set of 128 spectral measurements, *i.e.* 128 measures of intensities in limited spectral domains centered around given wavelengths. Pixels are acquired sequentially along two spatial directions, so the resulting data set is an image cube with two spatial dimensions and a spectral one.

This section, like the rest of the document, exposes only what is required to understand the calibration process. More detailed information about the instrument's general concept can be found in the technical article included in the data base (files TECHNART.ASC or TECHNART.PS).

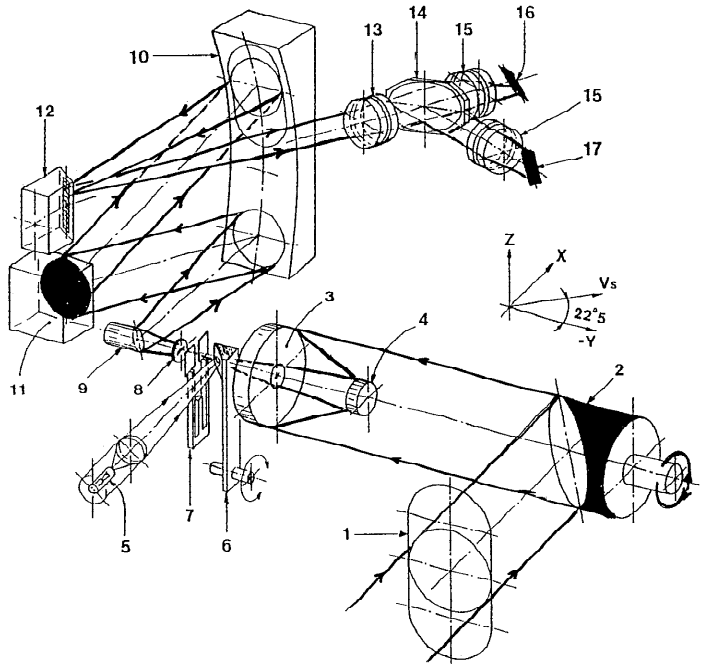

1 - Entrance Baffle
2 - Scanning Mirror
3 - Primary Mirror
4 - Secondary Mirror
5 - Calibration Source
6 - Tilting Mirror
7 - Modulator
8 - Entrance Slit
9 - Folding Mirror
10 - Parabolic Mirror
11 - Grating
12 - Field Mirror
13 - Entrance lenses
14 - Beamsplitter
15 - Imaging lenses
16 - 1.6 to 3.2 μm detector
17 - 0.8 to 1.6 μm detector

Figure 1: Optical Scheme

Imaging system

ISM uses a whiskbroom concept: longitude scanning is obtained with the motion of the

spacecraft on its orbit; the other spatial dimension is scanned by a one-axis mechanism; a complete spectrum is acquired at each time step. The viewing direction of the instrument is normally anti-solar when the spacecraft is stabilized. The scanning mechanism consists in an entrance mirror moving around this rest position by steps of 1 arc minutes. The mirror turns around the Y-axis of the instrument (the optical axis of the telescope) and allows an excursion of ±20° from the anti-solar position along the Z-axis (Fig. 1). The projection of this scanning axis on the surface of Mars was tilted on the Martian equator by an angle of about 45° at the time of observation. The precise value is a function of the angle between the equatorial plane and the solar direction, and thus changes during the Martian year.

The image supplied by the telescope is modulated and then enters the spectrograph through a slit elongated in the X-direction, *i.e.* perpendicular to the mirror scanning direction.

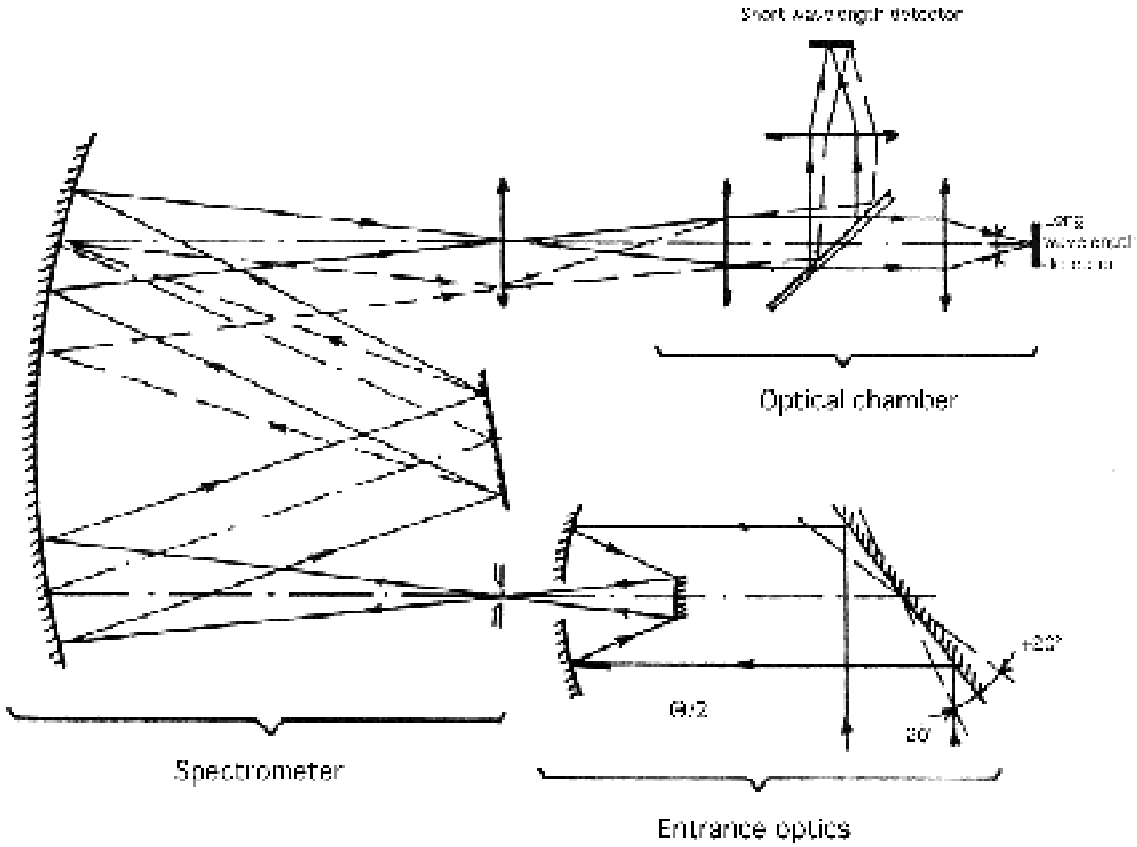

Figure 2: Principle of the optical system

Spectrometer

The scattering system is a grating spectrometer (Fig. 2). The first two orders of the

grating are used so as to minimize the volume of the instrument, increase the luminosity and decrease optical aberrations. The first three orders of the grating actually overlap in the domain that is used: information relative to different wavelengths are mixed in a given direction of reflection from the grating, and must be separated (Fig. 3).

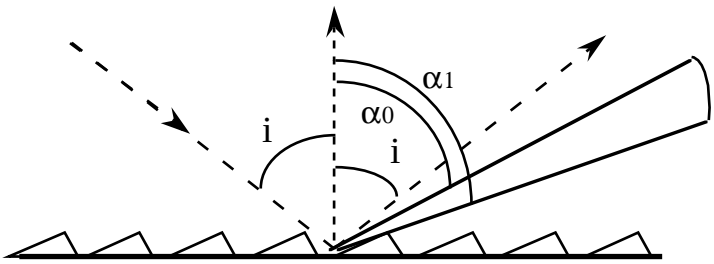

The angular domain used ranges from α_0 to α_1.

This corresponds to the scattering direction of wavelengths:

- 1.6 to 3.2 μm in the first order
- 0.8 to 1.6 μm in the second order
- 0.53 to 1.07 μm in the third order

Figure 3: Grating orders overlap

Optical chamber

The three spectral orders are separated as well as possible by optical methods before reaching the detectors (Fig. 4). This is done by using:

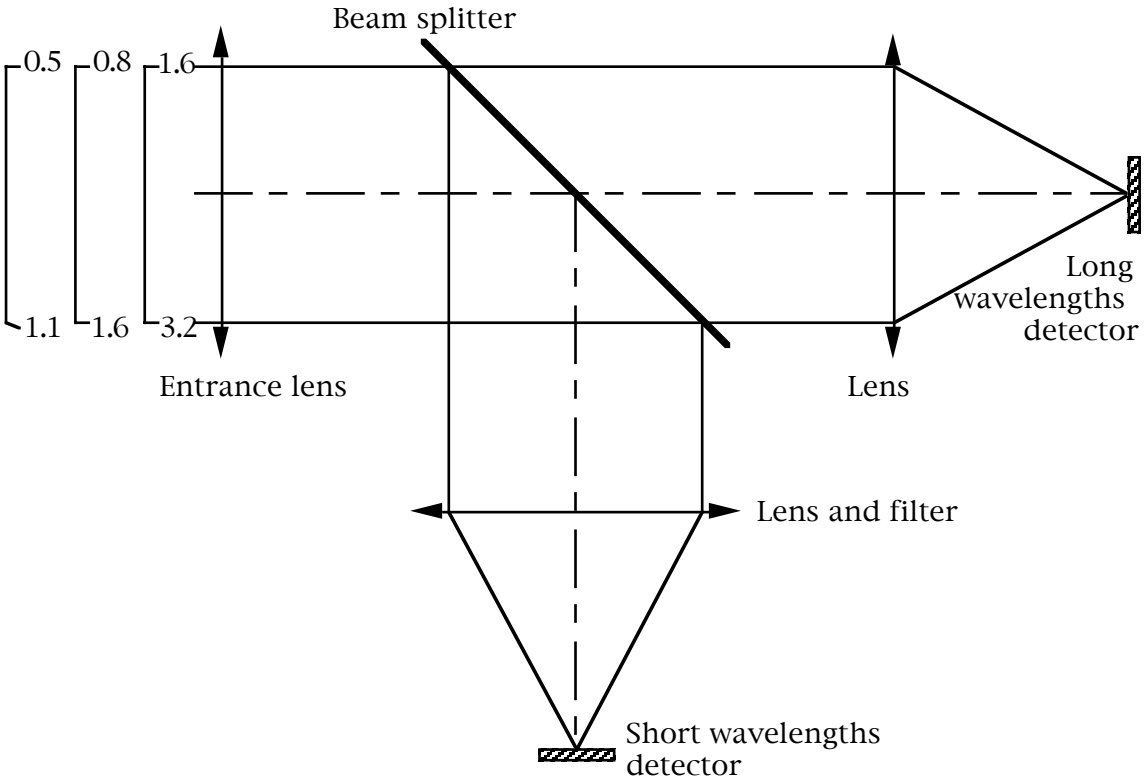

Figure 4: Optical chamber

1) A beam-splitter, transmitting above 1.6 µm, reflecting below. It separates the two spectral ranges, long and short wavelengths, corresponding to the first two orders.

2) A filter transmitting only above 0.8 µm, so as to eliminate the third order contribution in the short wavelength range.

The optical characteristics of the filters are such that:

- the beam-splitter is completely reflecting below 1.6 µm, so that only light of the expected wavelength reaches the detectors in the long wavelength range (Fig. 5b).
- in the short wavelength range, most of the light outside the nominal spectral range is filtered. However, two other contributions reach the detectors: first, the reflection of the beam-splitter is not completely null above 1.6 µm (Fig. 5a) so some photons scattered in the first grating order are not filtered; second, the third order cannot be filtered above 0.8 µm without affecting the second order information, and contributes to the measured intensity.

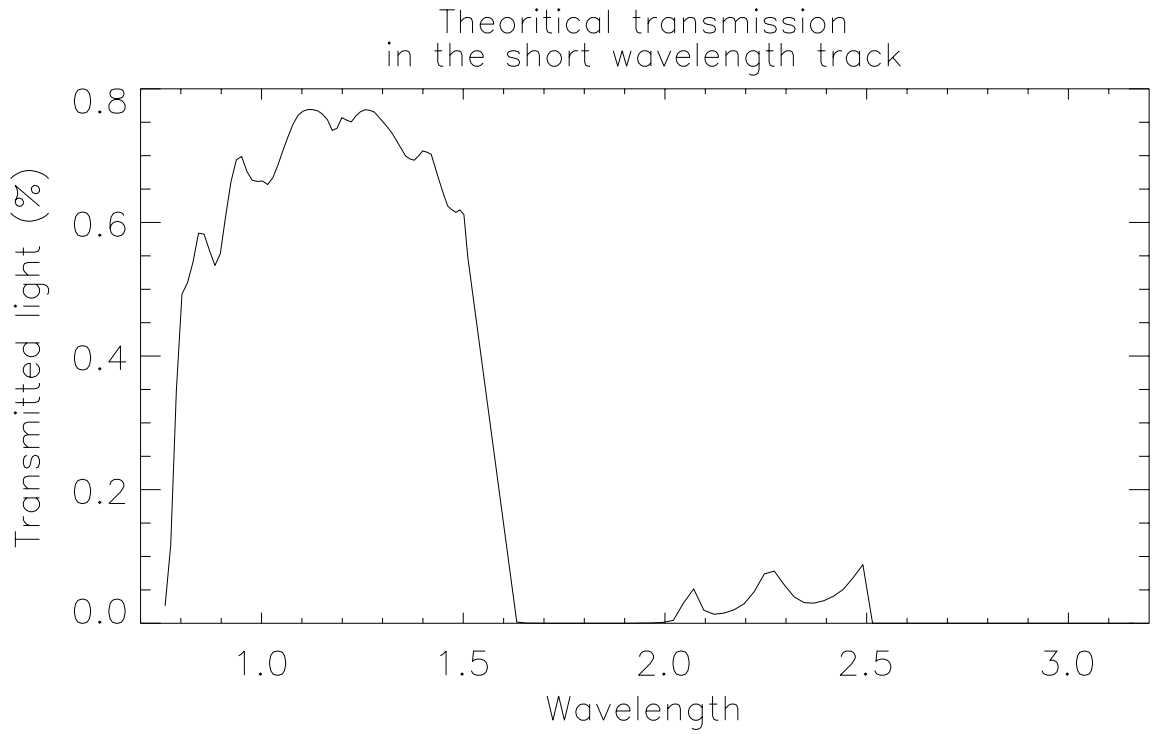

Figure 5a: Instrument's transmission
(measurements stop at 2.5 μm)

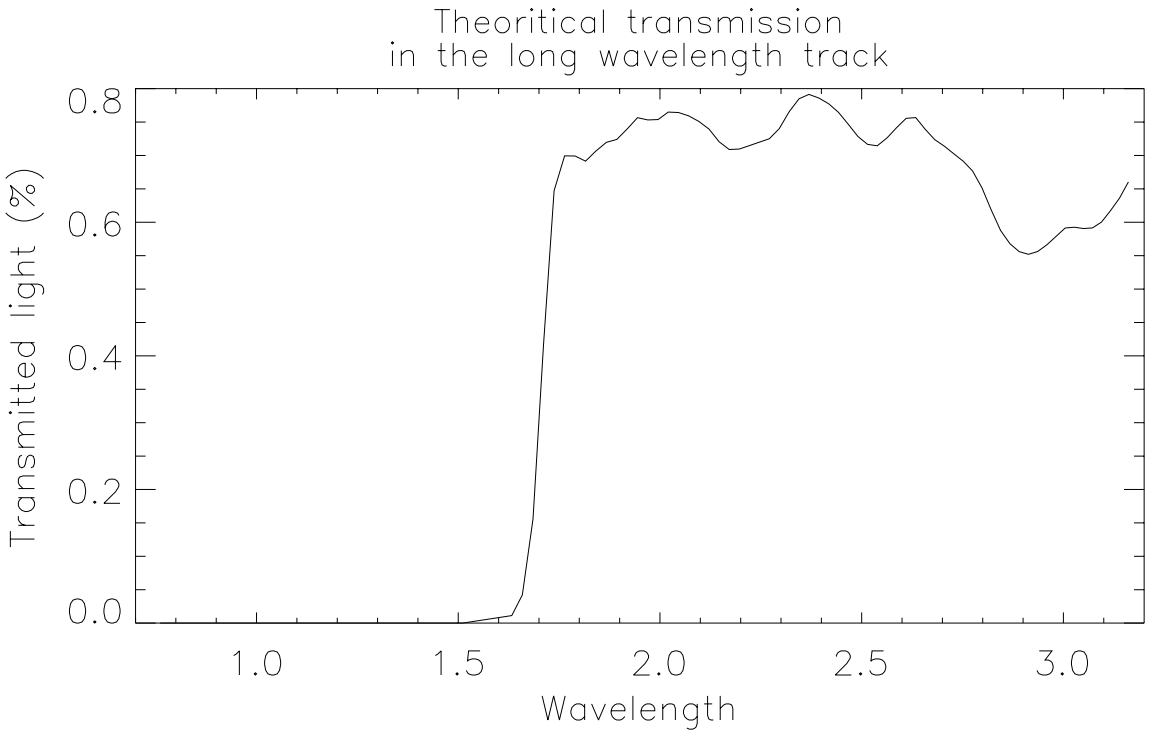

Figure 5b: Instrument's transmission.

Impulse response

If the entrance signal is a monochromatic beam, the output of the instrument can consist of zero, one or two peaks depending on the input wavelength. Five spectral domains can be distinguished on this basis (Fig. 6).

Detected signal

Conversely, if the input signal $I(\lambda)$ is spectrally continuous the signal incident on the detectors is, letting λ be the wavelength corresponding to channel Ch:

- In the long wavelength range, where $\lambda \in [\ 1.6\ ,\ 3.2\ \mu m\ ]$ and $Ch \in [\ 65\ ,\ 128\ ]$

$$S_{Ch} = I(\lambda)\ .\ \alpha_{Ch}$$

and the output is simply proportional to the signal.

- In the short wavelength range, where $\lambda' \in [\ 0.8\ ,\ 1.6\ \mu m\ ]$ and $Ch' \in [\ 1\ ,\ 64\ ]$

$$S_{Ch'} = I(\lambda')\ .\ \alpha_{Ch'} + I(2\lambda')\ .\ \beta_{Ch'} + I(2\lambda'/3)\ .\ \gamma_{Ch'}$$

where the three terms are respectively the second, first, and third order contributions to the signal in this range. The third term is null where filtering is efficient, *i.e.* where $2\lambda'/3 < 0.8$ µm (Fig. 7a).

The three coefficient sets α, β, and γ are related to the optical characteristics of the instrument, but also include spectral response of the detectors and pre-amplification coefficients corresponding to a nominal gain of 1 (see section "On-board processing"). The estimates given in Fig. 7 are computed from optical characteristics only.

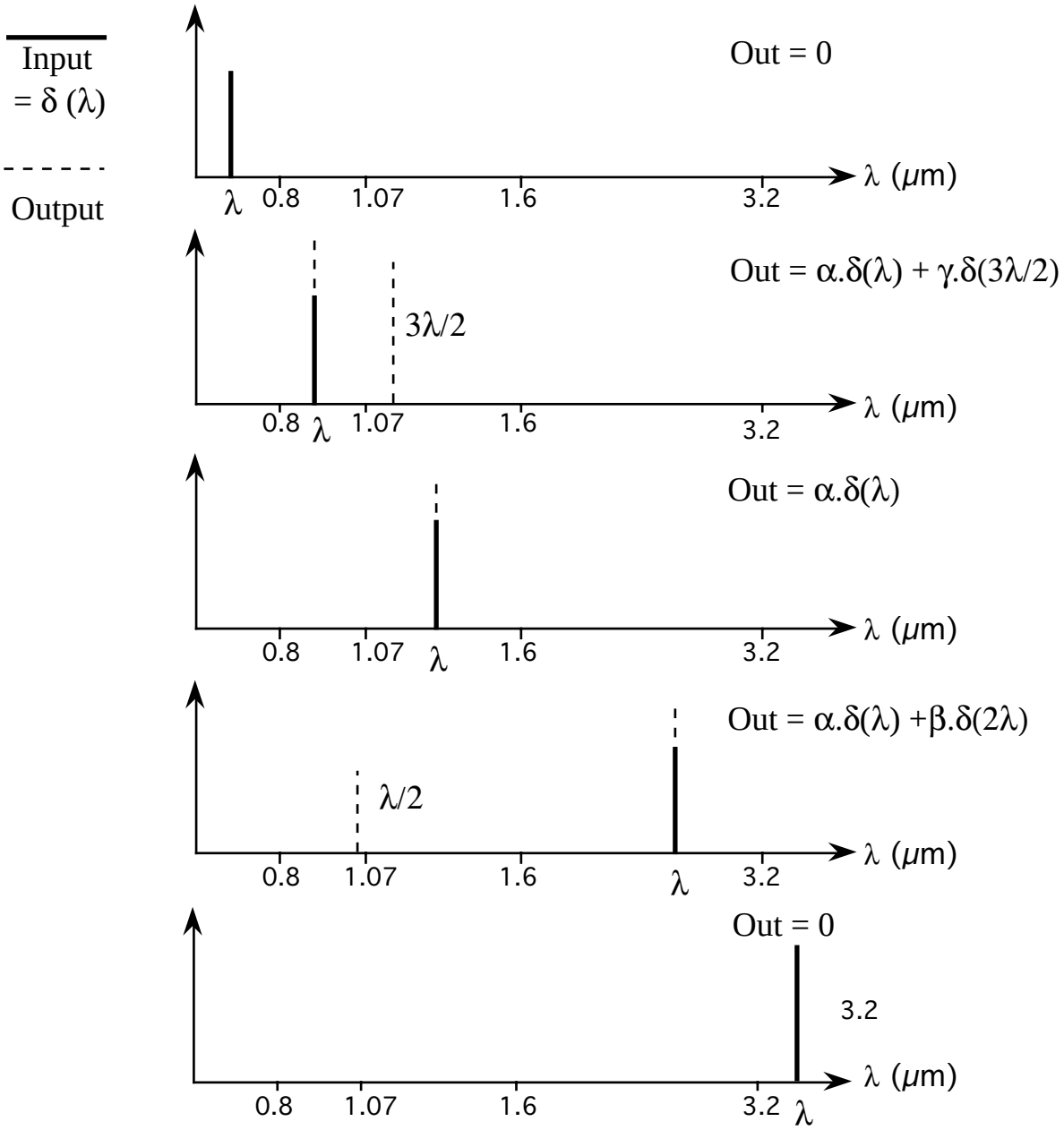

Figure 6: Impulse response

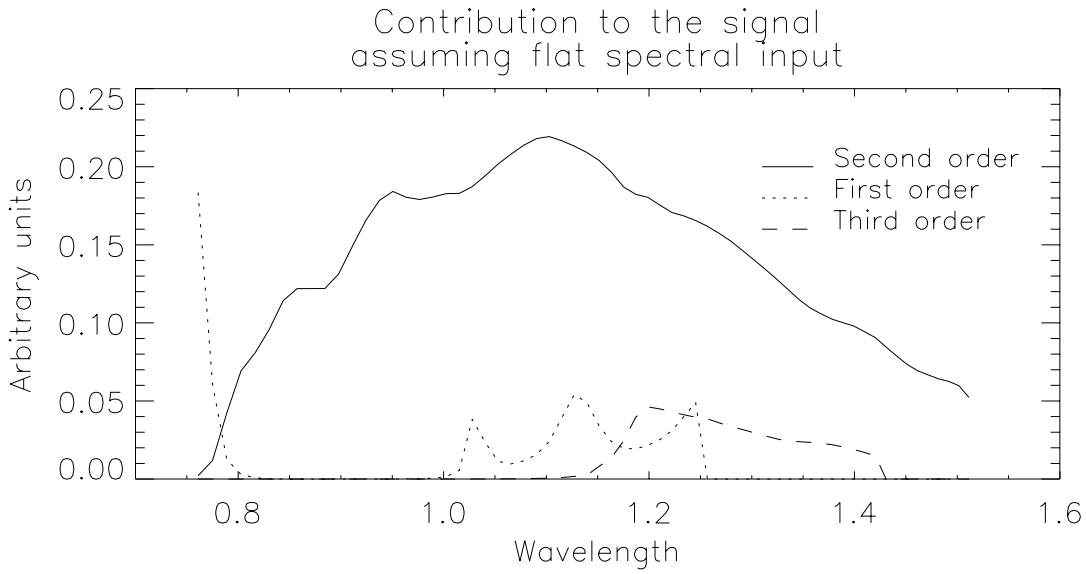

Figure 7a: Contributions of the three orders to the signal

Relative importance of the contributions

In the short wavelength range, α is about four times larger than β and γ (Fig. 7a). These values would directly apply for a spectrally flat input signal. However the actual input is basically an attenuated solar spectrum, and in this spectral range $I(2\lambda'/3)$ is larger than $I(\lambda')$, which is in turn much larger than $I(2\lambda')$. As a result, if the first order contribution is small with respect to the "direct" signal (from the second grating order in the short wavelength range), the third order contribution cannot be neglected (Fig. 7b): when looking at a completely reflecting surface lit up by the Sun, the maximum contributions of first and third orders at a given wavelength are respectively of 3 and 10% of the second order radiance measured at the same wavelength. The deconvolution of these three contributions is therefore an important step in the reduction process.

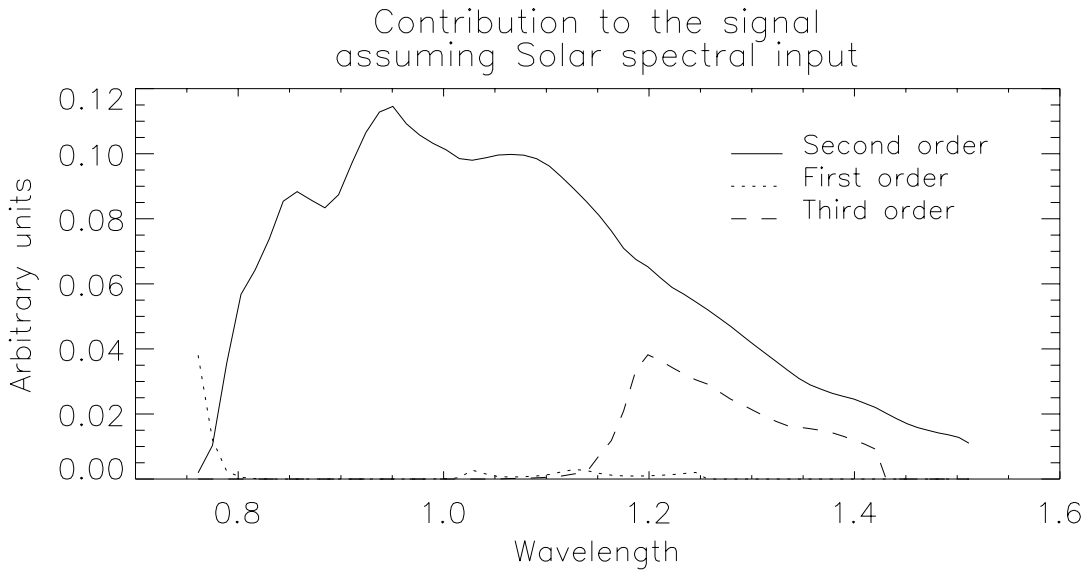

Figure 7b

Stray light

A certain amount of light coming from outside the nominal field-of-view of 12' also contributes to the measured signal. This contribution comes from a solid angle estimated to be at least 20° in size. On Mars this corresponds to a region of ≈2000 km, large enough to have constant spectral properties in any point of the disk.

The magnitude of this effect has been estimated by using the first observation track on Phobos, acquired while the satellite was passing between the spacecraft and Mars. In these spectra, atmospheric features of Mars are observed at 2.0 μm. The magnitude of this contribution can be estimated knowing the respective albedos of Mars and Phobos and the depth of absorption in the Martian spectra. When looking at a uniformly bright field the 20° area surrounding the field of view contributes to about 2% of the signal at 2.0 μm. Observations of the dark sky near the limb of Mars provide other estimates of this effect.

Altogether, the stray light acts like a wavelength-dependent, additive background,

reducing the spectral contrast of the Martian surface and producing systematic features in the uncorrected spectra. This doesn’t degrade spatial resolution, but decreases spectral contrast. This problem is handled through a linear recalibration of the data (see section “Correction process”). For observations of Phobos against the dark sky, the stray light is assumed to be negligible. The effect is not known with such accuracy as to make it possible to correct observations of Phobos with Mars in the background.

Electronics and on-board signal processing

Detectors

The two separated ranges, for short and long wavelengths, are measured independently by two devices organized in two staggered rows of 32 individuals PbS detectors (see section “Detectors and viewing geometry”). The physical principle used is the decrease in resistivity of PbS detectors with illumination. The release time of this effect is much smaller than the shortest integration time (1/8 s), so that measurements are completely independent.

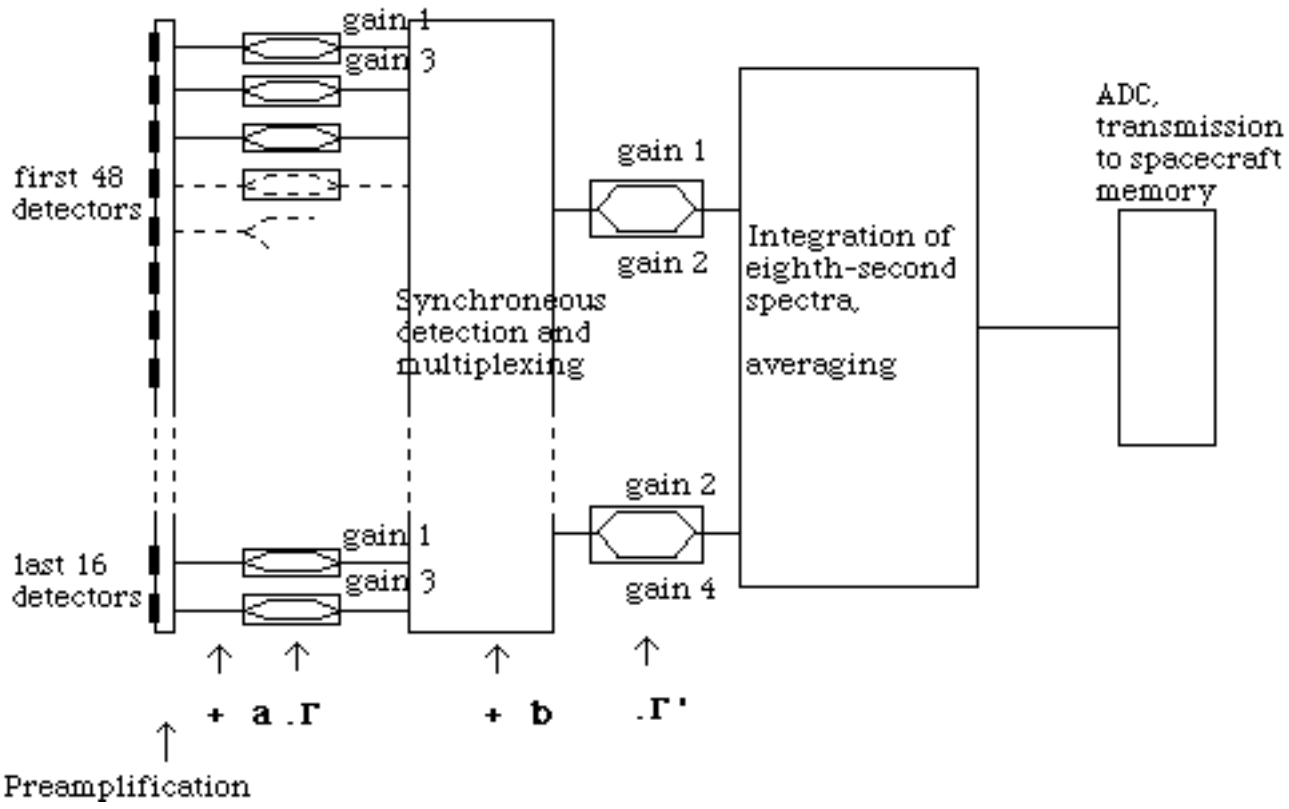

Figure 8: Electronic diagram

Acquisition

An initialization sequence is sent to the instrument before each session of observation. It

sets parameters such as starting time, observation mode and initial mirror angle, that determine the area to be observed, and other parameters related to on-board processing including integration time (τ) and two analogic gains (Γ and Γ'). A default mode is used when this information is not available. The detectors are read every eighth second whatever integration time is chosen. The signals are pre-amplified immediately after acquisition (Fig. 8), which results in the addition of a specific offset (a).

A first step of processing consists in amplification of the 128 signals, synchronous detection and multiplexing. A first amplification gain (Γ) is applied independently (in parallel) on the 128 channels. Two nominal values can be chosen: 1 (direct transmission), or 3. In this case, the actual value is closer to 3.5, and is specific to each channel (see Fig. 9).

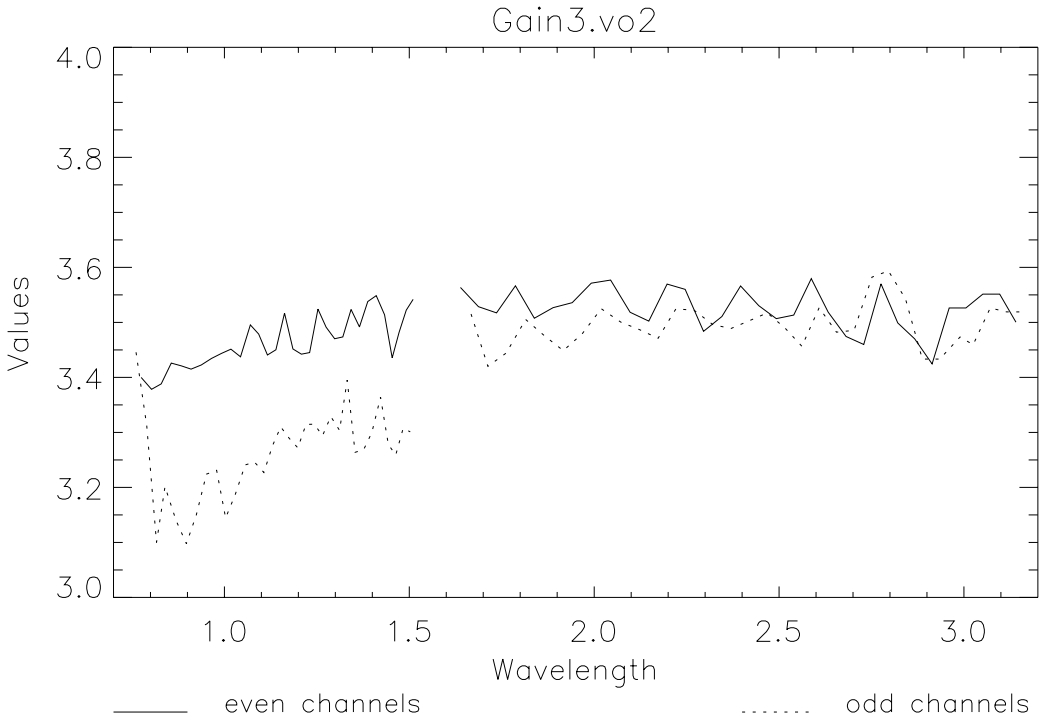

Figure 9: Gain 3 coefficients

A second level of processing is performed in another part of the instrument, and is performed in sequence for various groups of channels. Since the signals must be stored during this operation, a second offset (b) is added in this second step, the value of which depends on

the channel. A second amplification gain (Γ') can also be selected in the initialization sequence. In the gain-1 option, the first 48 channels of each devices are transmitted directly (without amplification), the last 16 channels being amplified by a factor of approximately 2. In the gain-2 option, the coefficients are respectively of about 2 and 4. The various gains used in this step can be considered independent of the channel. Gain 1 is assumed to be exactly 1, *i.e.* it is included in the transfer function α. The over-amplification of the last channels of each device compensates the decrease of the intensity along the spectrum (which is basically a solar spectrum), and minimizes the digitization noise. Similarly, a difference of amplification exists between the two ranges which also compensates the drop-off of the reflected spectra toward the long wavelengths; its value is also included in the transfer function, and does not appear explicitly in the correction process.

Last, the eighth-second spectra are digitized on 12 bits, and finally averaged during the integration time selected, so the output level doesn't depend on the integration time (conversely, it depends on the analogic gains selected); this insures that no saturation will occur at longer integration times. The electronic module of ISM eventually formats the data blocks, adds ancillary information, and transmits them to the spacecraft memory.

Output signal

The signal transmitted to Earth is:

$$O_{Ch} = [(S_{Ch} + a) \cdot \Gamma + b] \cdot \Gamma' ,$$

where a, b, Γ and Γ' depend on the channel, and where S_{ch} is the signal measured by the detectors, as detailed in the section "Instrument principle" (*i.e.*, the energy received from the various orders of the grating times detectors response). All offsets and gains depend on the detector temperature, which is monitored during observations (see section "Origin of corrections").

This output signal can be written

$$O_{Ch} = S_{Ch} \times \Gamma \Gamma' + DC_{Ch} ,$$

where DC is the dark current (output of the instrument when looking at the dark sky), which can be measured separately and afterward subtracted from the signal.

The linearity of the instrumental response is better than 1% for correct input signals and gains (DN output from 0 to ≈3800). In one session acquired at gain 3 (the western part of the

Ascraeus image cube) some channels reach saturation or non-linearity levels in the brightest areas (mainly channels number 10, 14, 18, plus channels 22 and 23 on a few very bright spectra, and at least odd channels 70, 72, 74 and 76 in the long wavelength range).

Signal-to-noise ratio

The fluctuations where estimated from the flight data, using the calibration sessions to measure those of the dark currents, and normalized spectra of bright homogeneous regions of Mars to measure those of the signal. The corresponding standard deviations are given in Table 1.

(in digits)	σ_{DC}	σ_{sig}	$\sigma_{total} = \sqrt{\sigma_{DC}^2 + \sigma_{sig}^2}$
gain 1	0,32	0,64	0,71
gain 2	0,54	1,02	1,15
gain 3	0,87	1,50	1,73

Table 1: Signal to noise ratio at various possible gains

These values are constant along the spectral domain, with no correlation to the magnitude of the signal. At gain 2 or 3, the digitization noise is negligible (the noise is proportional to the gain) and the sensitivity of the experiment is limited by electronic noise. For observations at gain 1, the digitization noise becomes more important.

The signal to noise ratio of the experiment is thus:

$$\frac{S}{N} = \frac{S_{Ch} \times \Gamma\Gamma'}{\sqrt{\sigma_{DC}{}^2 + \sigma_{sig}{}^2}}$$

For typical observations of Mars (window mode at gain 2, integration time of 0.5 s) this ratio varies from 200 to 1500 and becomes lower than 100 above 2.7 µm. Fig. 10 shows the average signal-to-noise in the Syrtis-Isidis image cube. The ratio in the short wavelength range is far lower for the odd channels, possibly due to a poor alignment of the device relative to the image of the slit. In the Phobos image cube, the signal-to-noise varies from 30 to 300. Scientific results imply that the noise is actually a little overestimated.

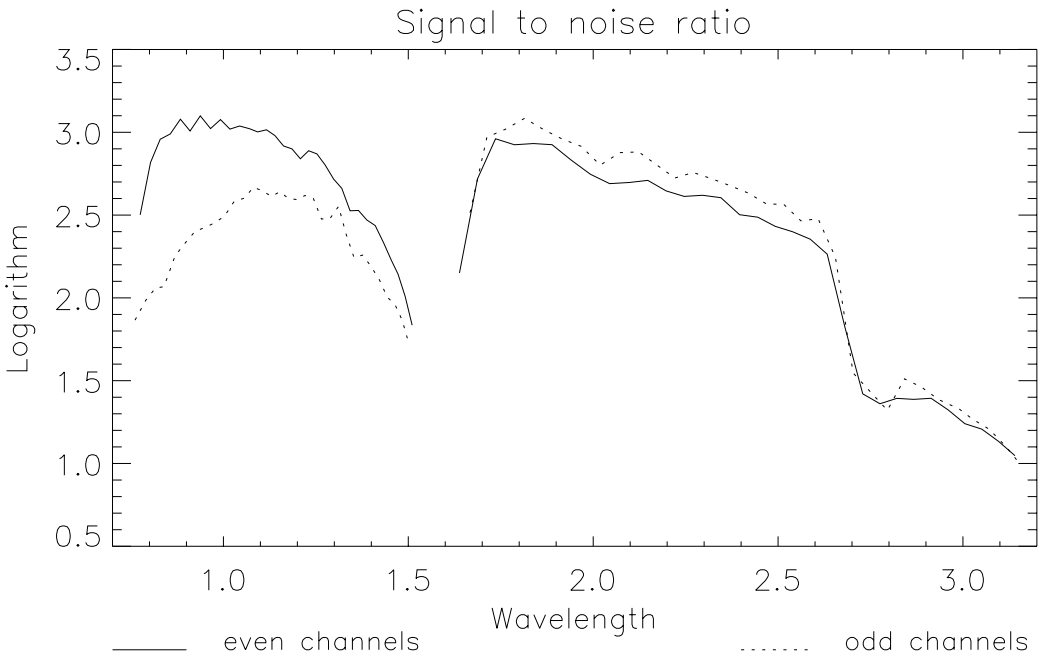

Figure 10: Logarithm of signal-to-noise ratio
in the Syrtis-Isidis image cube

Detectors and viewing geometry

Similar devices are used in both spectral range. Each device is an array of 64 individual detectors in two staggered rows, which we term odd and even rows. This particular design is related to the wiring of individual detectors. The relative location of the detectors is detailed in Fig. 11. The size of the detectors, together with optical aberrations, defines both the pixel size and the spectral step of the instrument. Note that the appellations “odd” and “even” are not related to channel numbers, but to the identifier of the telemetry block containing the information (see Table 2). Channels are numbered in sequence of increasing wavelength.

Viewing directions

The angular size of a region seen by one detector (a pixel) is about 12’ taking into account the aberrations of the system. As a first approximation, in each of the four rows of 32 channels all detectors look in the same direction, *i.e.* they all see the same region at a given time. The two arrays are aligned across the image of the slit with good accuracy, so the possible discrepancy between the two extremities of an array is very small. The relative location of the two arrays with respect to the optical parts is not so accurate however, which results in a small difference in viewing direction between channels of same parity in the two arrays: images acquired by even (or odd) pixels in different spectral ranges are shifted by less than one pixel (≈9’, see Table 2) along the slit (across the scanning direction), and can be matched as described below.

Last, the odd and even rows of each array are also shifted in the perpendicular direction, and hence they see different parts of the image of the slit. This results in a discrepancy in viewing direction that is on the order of two pixels wide (≈21’, see Table 2).

Range, row	Channel set	Angular shift along the slit
Short wvlgth, odd	{ 1, 3, 5,…, 63 }	-0.15° = -9’
Short wvlgth, even	{ 2, 4, 6 …, 64 }	0.20° = 12’
Long wvlgth, even	{ 65, 67 …, 127 }	0.34° = 20.4’
Long wvlgth, odd	{ 66, 68, …, 128 }	0° = 0’

Table 2: Angular shifts between the four rows

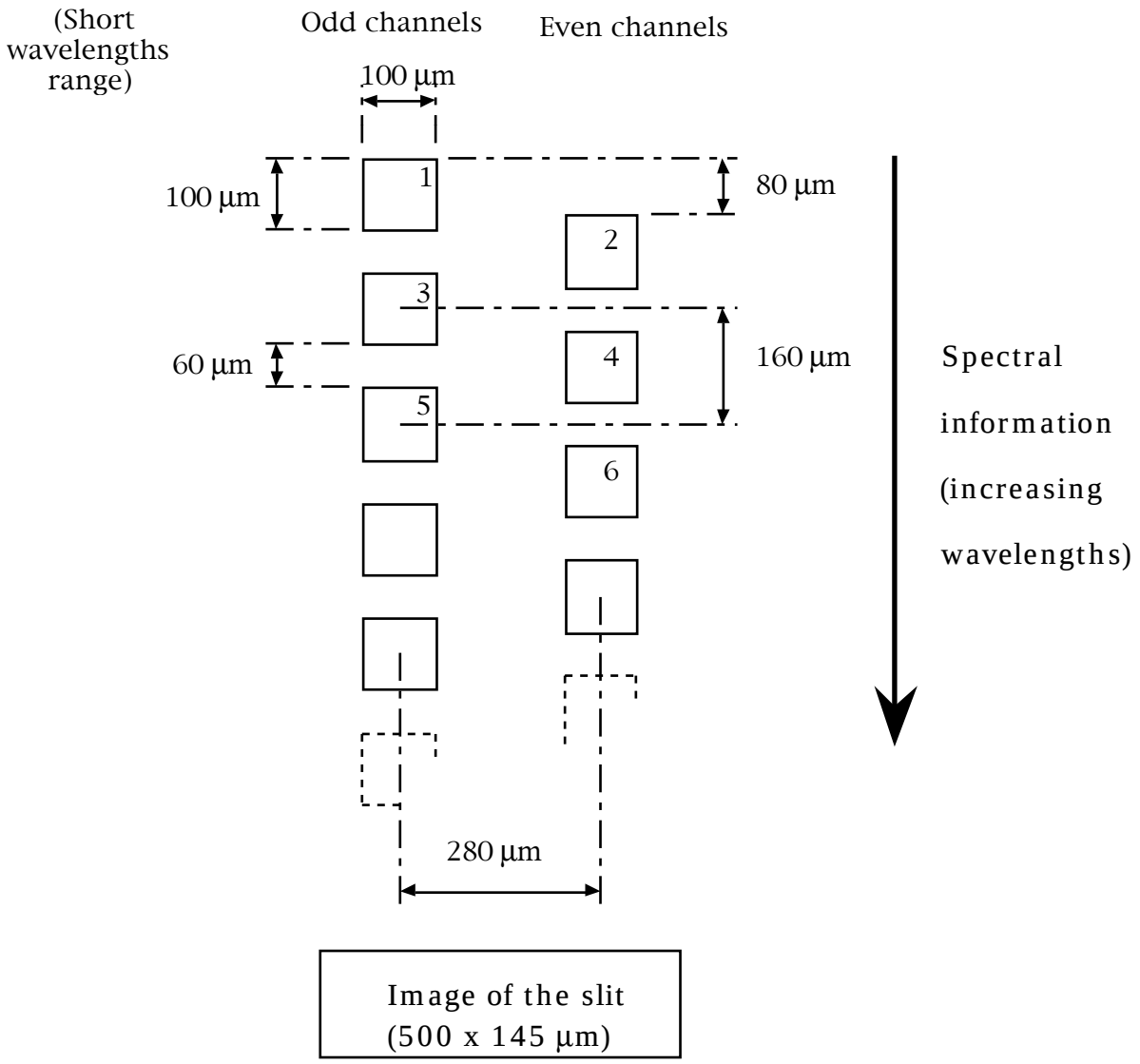

Figure 11: Location of the detectors in the focal plane. The image of the slit is the projection of the X-axis of the instrument, perpendicular to the scanning direction. 160 μm correspond to a field of view of 12 arc minutes, taking into account the aberrations.

Computing the coordinates

The Fortran program COORD.FOR computes the pixels coordinates for the 11 sessions on Mars and writes the files *_COOR.DAT. Coordinates of the pixel centers are computed from orbital parameters on the day of observation, knowledge of the attitude of the spacecraft, position of the entrance mirror, and time. Coordinates are then globally shifted (by ≈0.5°) to refine the match with Viking and Mariner 9 altimetry maps. The coordinates corresponding to the four corners of the pixels are computed similarly from the location of the detectors in the focal plane. Viewing angles (incidence, emergence and phase) are also computed and stored in

the same files. Coordinates are written for channels in the short wavelength, even row, although the program can optionally compute the projection of channels from the other rows, using the angular differences given in Table 2. This program will work only for observations of Mars when the spacecraft is 3-axis stabilized, either on a circular or an elliptic orbit. The accuracy is on the order of the pixel size (≈0.5°).

Coordinates for the Phobos image were derived by comparison with an image acquired at the same time by the spacecraft camera (VSK) and with Tom Duxbury's digital model of Phobos. The Phobos coordinates are given (together with viewing angles) as latitude/longitude in the file PHO_COOR.DAT, and as Cartesian coordinates in the image plane in the file PHO_SCRN.DAT (see file SOFTINFO.TXT for use of these files). Those values also correspond to the short wavelength, even pixels.

Registration of spectral ranges

Because of the large difference in viewing directions, the different rows of detectors do not see exactly the same spot on the surface and should be registered. On the 11 Mars sessions however, the spectra can be recovered easily in first approximation: the long and short wavelength ranges are shifted by nearly one-pixel along the slit direction with the short wavelengths acquired first, and the lines of pixels are adjacent to one another. In Fig. 12, short wavelengths information on pixel A and long wavelengths information on pixel C are acquired simultaneously. The complete spectrum of pixel A can be recovered by shifting the two images (short wavelengths at line x/sample y and long wavelengths at line x+1/sample y-1). Similarly, the odd and even parts of the same spectral order can be merged directly using a 2-pixel shift: in Fig. 12, odd channels of pixel B and even channels of pixel C are acquired simultaneously, so the spectrum can be recovered by taking odd channels at line x/sample y and even channels at line x+2/sample y-2.

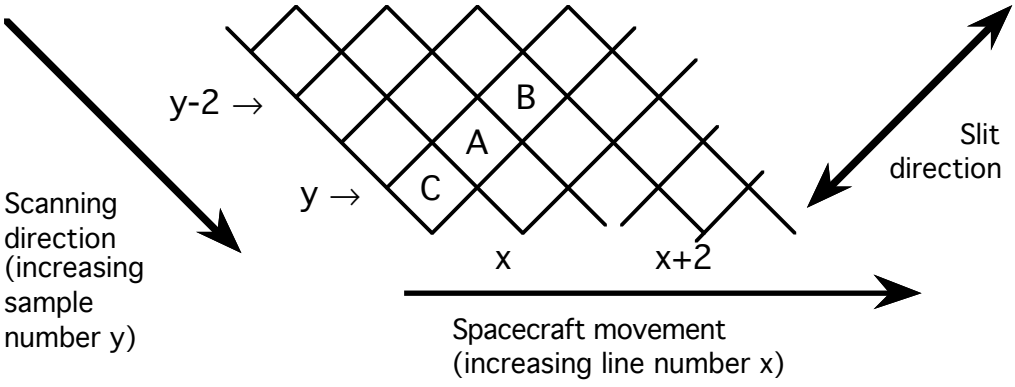

Figure 12: Scanning in window mode.

This method is only an approximation: the long wavelengths information corresponding to pixel A is more a weighted average from spectra at x/y and (x+1)/(y-1) (about 25% and 75%, although the exact figure depends on geometry and thus changes between and within sessions). On high-resolution sessions on Mars, the approximation is rather good. On the Phobos image cube however, the surface is scanned from east to west so the long wavelength/even channels information is acquired first and the method would not work directly.

Registration of spectral channels

An unexpected effect concerning viewing directions was detected during data analysis: two neighbouring detectors do not look exactly in the same direction, and therefore see slightly different spots on the surface. Two phenomena combine to produce this effect. First, the small error of alignment of the arrays relative to the image of the slit results in a slow drift of the pixel projection with channel number. Second and more important, the sensitive coating of the detectors is not perfectly homogeneous: the most sensible region is randomly distributed on the detector, which causes a discrepancy in pointing direction between two consecutive channels. This misregistration between channels amounts to a few tenths of pixel (<6').

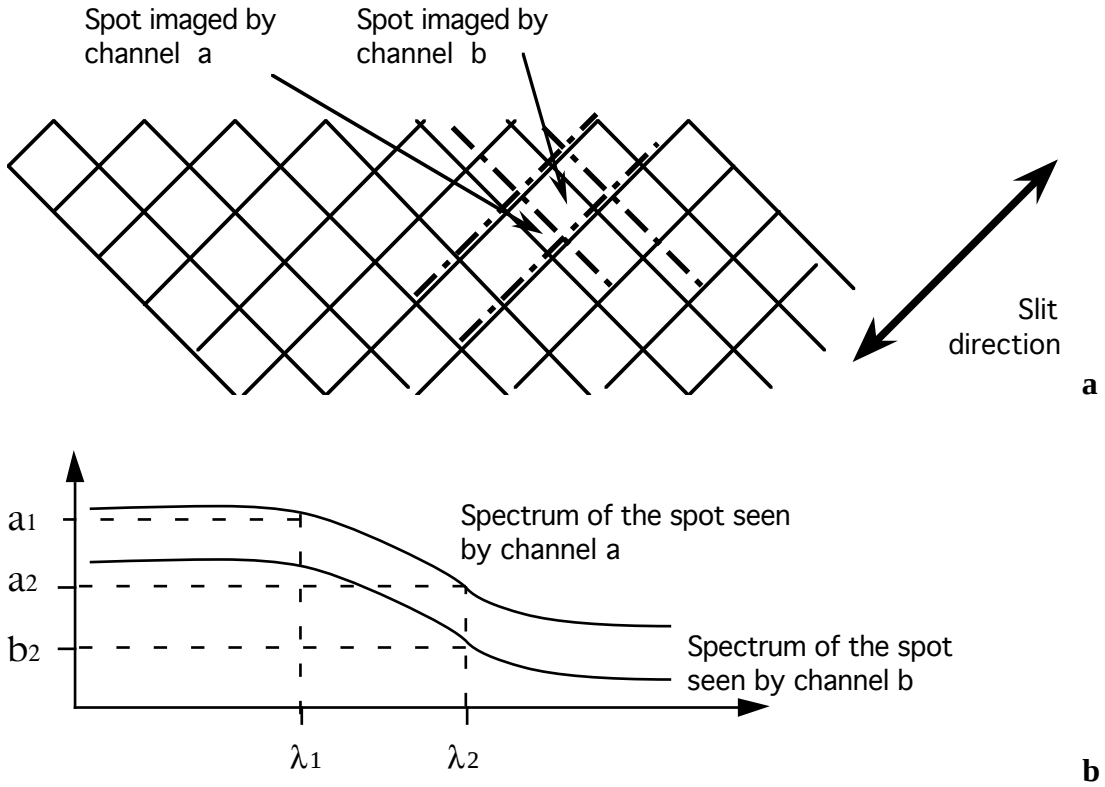

Figure 13: Misregistration effect

Therefore two channels in the same row do not see exactly the same spot on the surface (Fig. 13a). This problem is most significant along sharp albedo boundaries (strong reflectance gradient across the scanning direction), where two channels look at areas having slightly different coverage by bright and dark materials. Ratios of intensities in two channels may result in a sort of "edge effect": in Fig. 13b, the ratio of intensities at λ_1 and λ_2 is a_1/b_2 instead of a_1/a_2, which yields in this case an overestimate of the spectral slope.

An empirical correction of this effect was derived from ground calibrations. The shifts between channels images were measured from observations of a spatially structured scene, and are stored in the file DECAL2.DAT (Fig. 14). These coefficients are then used to perform a 3-pixel convolution on the spectral images. Each intensity is replaced by a weighted mean of the adjacent pixels along the slit:

$$O_{Ch'}(l,s) = O_{Ch}(l,s) + \frac{\delta_{Ch}\left[O_{Ch}(l+1,s-1) - O_{Ch}(l-1,s+1)\right]}{2}$$

where $O_{Ch}(l, s)$ is the output in channel Ch for the pixel at line l and sample s,
$O_{Ch}'(l,s)$ is the same quantity corrected for the registration effect,
δ_{Ch} is the weight coefficient corresponding to channel Ch.

Wherever one of the neighbouring pixels is missing the procedure is adapted accordingly; wherever the central pixel is missing it is interpolated from the two neighbouring pixels; wherever only the central pixel is present it is kept uncorrected; otherwise the information cannot be recovered.

This correction is performed by the program ETALONNE.FOR on the eleven Mars sessions. It is applied after correction of telemetry errors to avoid propagating them to adjacent pixels, as the first step in the calibration process (before subtracting the dark current, to remain consistent with the procedure used to derive the coefficients). The correction slightly downgrades the spatial resolution and the dynamic of the data, but is efficient in most cases and provides a good interpolation of the holes in the images. It can be inappropriate where the reflectance gradient varies on a one-pixel scale. In a few occurrences where the sub-pixel variations of the gradient are large (mainly along the northern border of Valles Marineris) the correction may result in a double "edge effect". The maximum remaining error in spectral ratios after correction is on the order of 2%, and is localized in these narrow areas. This error is large enough to result in significant damage to a number of spectra covering both the canyon floors and the plateau in the VMC image cube, however.

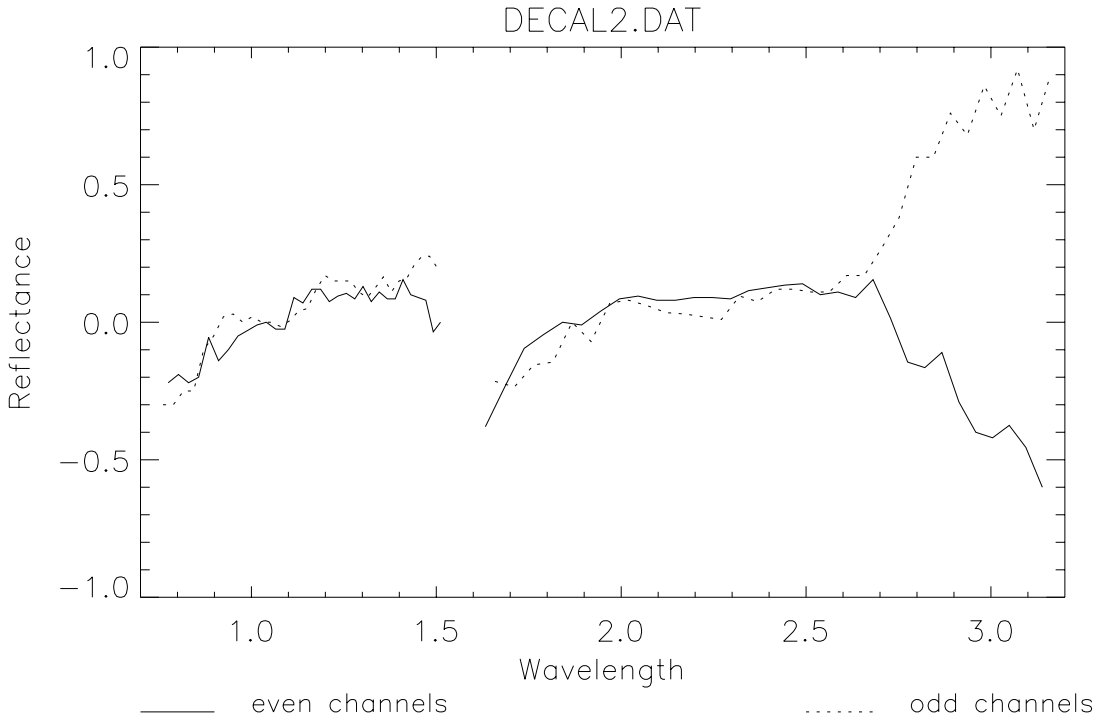

Figure 14: Coefficients for registration correction

The different geometry for the Phobos image cube requires a slightly different method: a 3-pixel convolution is applied with the same coefficients, using the nearest neighbours in the image plane. This resampling is performed by CORPHO.FOR, and the resulting values are written in an intermediate data file (PHOEVEN.RES and PHOODD.RES). This step of processing is even more critical for Phobos than for Mars, due to the very small spectral variability in the image cube, so this resampled data should be considered as the primary data for Phobos.

Spectral calibration

Correspondence between channels and wavelengths

The exact channel-to-wavelength correspondence depends on the actual alignment of the detectors with respect to the optical parts, and must be measured. This calibration was performed using a monochromatic source, the spectral resolution of which was about ten times that of ISM. A response curve was obtained as a function of wavelength for each channel, with the maximum detectivity giving the nominal wavelength for this channel (see Table 3). The complete response for each detector is given in files REPONSES.DAT (even channels) and REPONSESI.DAT (odd channels) and can be plotted by the IDL routine AFFREP.PRO. The fortran program LECSPE.FOR uses the overall response curve to integrate any spectrum to ISM spectral format, provided that the spectral resolution be at least that of ISM.

Measurements with the monochromator cannot be used to compute the transfer function α, because the incident flux from the source was neither controlled nor monitored. They cannot be used either to measure the contributions from first and third orders in the short wavelength range (β/α and γ/α), because the source actually provides several harmonics in addition to its monochromatic beam: secondary peaks in the calibration spectra are due both to ISM spectral overlap and to the monochromator itself.

Channels widths

The file LARGEURS.DAT gives an estimate of the channels width at half-height, as they were measured with the monochromator (Fig. 15); the average values are 20 nm in the short wavelengths and 50 nm in the long wavelengths. These values depend on the location of the devices in the focal surfaces, on the shape of those surfaces and on the homogeneity of the sensitive coating. The focal surface is not plane in the short wavelength range, and therefore the spot corresponding to a detector does not have a regular size along the spectrum (Fig. 16); the detector array is located so as to minimize the average distance to the focus. Heterogeneity in the sensitive coating result in a slight shift of the maximum detectivity of a given channel; this problem is similar to the misregistration effect, acting in this case in the spectral dimension of the device (*i.e.* across the slit) instead of the spatial dimension.

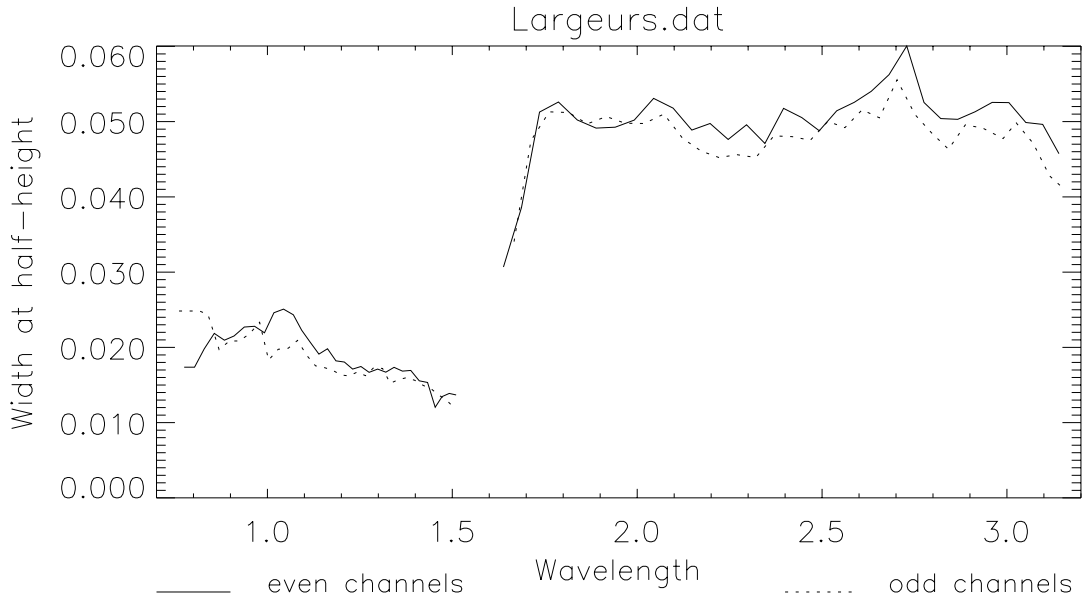

Figure 15: Channels' bandwidth

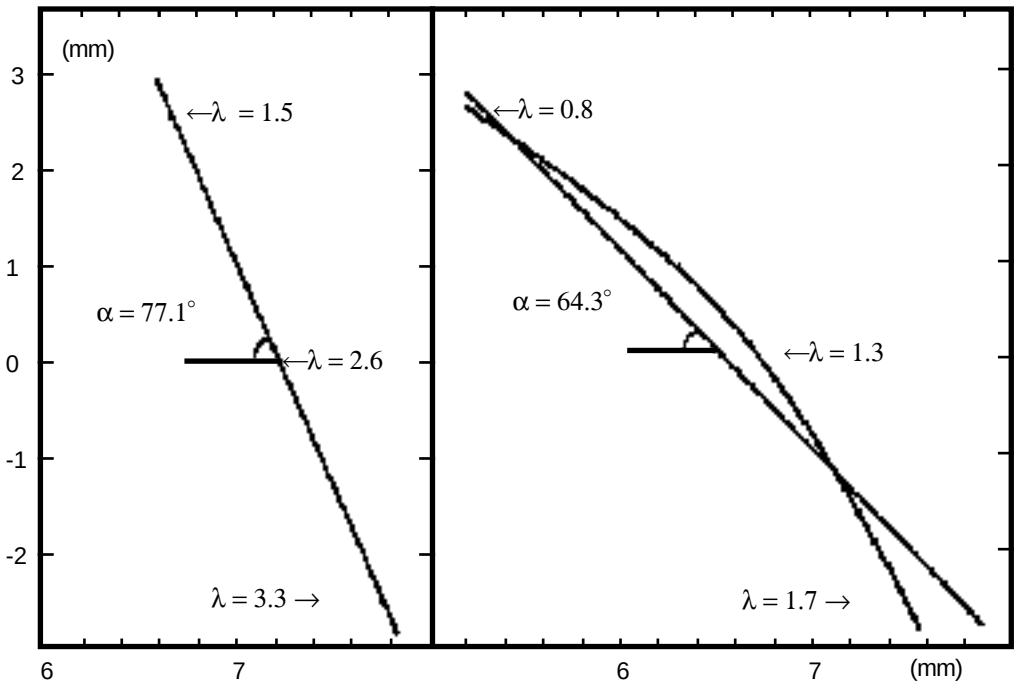

Figure 16: Focal surfaces. Distance in mm is counted from the last lens.

Channel number	Even channel	Odd channel	Wavelength	Channel number	Even channel	Odd channel	Wavelength
1		1	0.7610	33		17	1.1754
2	1		0.7750	34	17		1.1852
3		2	0.7900	35		18	1.1986
4	2		0.8029	36	18		1.2083
5		3	0.8165	37		19	1.2207
6	3		0.8292	38	19		1.2304
7		4	0.8394	39		20	1.2431
8	4		0.8564	40	20		1.2529
9		5	0.8695	41		21	1.2653
10	5		0.8837	42	21		1.2751
11		6	0.8973	43		22	1.2878
12	6		0.9099	44	22		1.2982
13		7	0.9239	45		23	1.3114
14	7		0.9375	46	23		1.3202
15		8	0.9514	47		24	1.3321
16	8		0.9653	48	24		1.3425
17		9	0.9790	49		25	1.3534
18	9		0.9920	50	25		1.3653
19		10	1.0033	51		26	1.3764
20	10		1.0177	52	26		1.3877
21		11	1.0292	53		27	1.3987
22	11		1.0436	54	27		1.4107
23		12	1.0560	55		28	1.4222
24	12		1.0701	56	28		1.4332
25		13	1.0815	57		29	1.4434
26	13		1.0926	58	29		1.4537
27		14	1.1067	59		30	1.4633
28	14		1.1163	60	30		1.4723
29		15	1.1301	61		31	1.4835
30	15		1.1393	62	31		1.4917
31		16	1.1523	63		32	1.5026
32	16		1.1627	64	32		1.5105

Table 3: Wavelength correspondence to channels
(short wavelength range)

The bandwidth ranges from 0.025 μm to 0.013 μm in the short wavelength range, while the spectral step in a given row (the distance between maximum of detectivity in two neighboring channels) is close to 0.028 μm. In the long wavelength range, the width and the distance between channels is of the order of 0.05 μm. Thus, when considering only channels in a given subset (odd or even), the spectral resolution of the instrument $\lambda/\Delta\lambda$ varies from 30 to 60 in both ranges, and spectral sampling is performed at half-Nyquist frequency.

Channel number	Even channel	Odd channel	Wavelength	Channel number	Even channel	Odd channel	Wavelength
65	33		1.6383	97	49		2.4453
66		33	1.6671	98		49	2.4681
67	34		1.6870	99	50		2.4925
68		34	1.7127	100		50	2.5157
69	35		1.7359	101	51		2.5397
70		35	1.7621	102		51	2.5617
71	36		1.7870	103	52		2.5872
72		36	1.8147	104		52	2.6083
73	37		1.8382	105	53		2.6330
74		37	1.8652	106		53	2.6552
75	38		1.8889	107	54		2.6811
76		38	1.9165	108		54	2.7028
77	39		1.9405	109	55		2.7290
78		39	1.9674	110		55	2.7512
79	40		1.9922	111	56		2.7756
80		40	2.0192	112		56	2.7957
81	41		2.0445	113	57		2.8210
82		41	2.0722	114		57	2.8419
83	42		2.0973	115	58		2.8668
84		42	2.1232	116		58	2.8875
85	43		2.1478	117	59		2.9138
86		43	2.1728	118		59	2.9344
87	44		2.1971	119	60		2.9600
88		44	2.2212	120		60	2.9895
89	45		2.2461	121	61		3.0053
90		45	2.2704	122		61	3.0248
91	46		2.2958	123	62		3.0511
92		46	2.3208	124		62	3.0710
93	47		2.3455	125	63		3.0966
94		47	2.3697	126		63	3.1153
95	48		2.3959	127	64		3.1406
96		48	2.4191	128		64	3.1576

Table 3 cont'd: long wavelength range

Origin of instrumental corrections

Recovering the input signal from spacecraft telemetry data implies correcting the various instrumental effects in sequence. This section contains information about the way we handle these successive steps, and possible remaining problems; the data reduction process itself is presented in section “Calibration procedure”. The correction is performed by several Fortran programs included in the data base (CONVERT.FOR, ETALONNE.FOR, CORPHO.FOR, ETALPHO.FOR and CORASC.FOR), and applied to the 11 main observations of Mars and to the image cube of Phobos. The 22nd February session on Mars is not calibrated, due to the difficulty to project the data on the Martian surface (see section “Observation sessions”); spectra from this session can be calibrated following the same lines, however.

Correction of telemetry errors

Some inconsistent records are found in the raw data files due to transmission losses, telemetry errors and cosmic rays incident on the detectors. A first check was performed by comparing the telemetry files received at two different ground stations. A cross-check between those two sets of files was performed by CNES, and provided the telemetry files included in the data base; although they occasionally contain repetitions, these files were not modified. The program CONVERT.FOR reads the files, decompresses science data and important ancillary information, corrects telemetry errors whenever possible, and writes the decompressed data as 16-bits integers. This program calls specific Vax Fortran routines to decompress the telemetry files and uses the Vax internal data representation, so its output must be considered as the primary data (see section “Structure of data block” for more information).

A spectrum is normally acquired at each time step in a two-dimension grid; however spectra can be absent or unusable. The continuity of the observations is restored in any case, with one record per sample in the acquisition grid, even when no information is available (the only exception is the systematic rejection of the first sample of each line in window mode, with no information written; see section “Observation modes”). Timing information, temperature measurement, and mirror position are always restored, and major errors in spectral measurements are corrected using a crossed checksum included in the telemetry files. Like the rest of the calibration process this step is optimized for even channels, while errors may remain

on odd channels. At this level some spectra are missing. Pixels with missing even block are always rejected and the corresponding record is filled with zeros. If good quality measurements exist on even channels, missing odd blocks may be interpolated from neighbouring pixels, so that all retained spectra have complete even and odd channels measurements.

This processing is applied to all observation sessions: the 11 image cubes on Mars and the Phobos image cube; all observations of Mars and Phobos with significant signal detected and detector temperature in the nominal range; all flight calibration sessions. The program makes it possible to extract any part of a telemetry file on a Vax system. The output files all have the extension ".EDT". Note that for calibration sessions the contents of the files is slightly different (see FILES.ASC or labels) and that no correction of telemetry error is applied.

Channels registration and interpolation

Registration of spectral channels is performed as described in section "Detectors and viewing geometry", as the first processing step in ETALONNE.FOR (Mars sessions), or in CORPHO.FOR (Phobos session). See section "Detectors and viewing geometry" for limitations of the procedure. This step doesn't apply to other observation sessions, in particular it shouldn't be applied to the 22nd February session on Mars, acquired when the spacecraft was spinning, since the pixels are not adjacent to one another.

Dark current subtraction

Dark current measurements are made twenty minutes before and after each session, as part of the in-flight calibration sessions. The detector temperature is thus very close to that measured during data acquisition. The gain can be different, since both analogic gains Γ and Γ' are selected independently for calibration and observation sessions. In any case, a dark current with the same gain and similar temperature is available for each image cube.

A constant dark current is always used for a given session, and this may result in a small remaining offset if detector temperature varies significantly during the corresponding acquisition session. The possible effect is very small however, and only one session is likely to be affected (March 7th, covering the central part of Valles Marineris, during which temperature varies from -76.6° to -78.0°). For the Phobos image the dark current could be integrated in the part of the image pointing at the dark sky; analysis of these spectra reveals that the signal is not uniform in the odd channels, however, but instead increases in the more eastern part of the image. This residual signal is probably due to an internal reflection related to the particular pointing geometry during this observation, and varies rapidly with longitude on Phobos. Even channels are only marginally affected however, and the dark current file for Phobos is taken

from the March 21st session (on the Ascraeus Mons area), also acquired at gain 3.

The dark current files to be used with each session are listed in section “Observation sessions”. The intensity in those files is already divided by 2 in the last 16 channels of each wavelength range to compensate amplification at the end of the devices.

Gain correction

This step consists of channel-by-channel division of the data by precise values of the analogic gain used during data acquisition. At gain 1 and 2, only two different values are used (one at the beginning and one at the end of the arrays); these four values were determined from ground calibrations and checked against flight data. The set of 128 gain 3 coefficients was determined from observations of the surface of Mars, using a relatively uniform region on Tharsis, east of Ascraeus and Pavonis Montes (file GAIN3.VO2). In this area, two locations distant by less than 400 km were observed at gain 3 on March 21st, and at gain 2 on March 26th. The ratio of these spectra provides the gain 3 coefficients for every channel. Some channels are saturated in spectra from the Ascraeus image cube, so the corresponding coefficients are interpolated. The accuracy of this correction is estimated to be better than 1% for even channels, but it is probably less accurate for the odd channels.

The resulting gains are used for the two image cubes acquired at gain 3, Phobos and Ascraeus (Fig. 9). They obviously do not correct for the saturation of some channels in the brightest spectra of the Ascraeus image cube (mainly channels number 10, 14, 18, plus channels 22 and 23 on a few very bright spectra, and at least odd channels 70, 72, 74 and 76 in the long wavelength range). Actual intensities in these channels are estimated through correlation with neighbouring channels for saturated pixels (correction performed by CORASC.FOR for even channels only). Another problem arises with these gains: the regular decrease at short wavelength in Fig. 9 is probably related to a different contributions of aerosols scattering between the two sessions. If so, the spectral slope is not directly comparable between Ascraeus and the other sessions; this is important in particular when studying aerosols properties or spectral slopes. On Phobos, the possible error in gain values is corrected by a specific transfer coefficients so it does not affect the calibrated data.

Detector temperature correction

The detectors sensitivity is a rapid function of temperature, with a maximum around -70° C. The focal plane temperature was therefore monitored and recorded during data acquisition every 14 s, with ≈0.05° accuracy. Variations of detectivity with temperature were calibrated on ground; however, cooling in space was more effective than predicted and the actual flight-

temperatures were lower by 10 to 15 K than expected before launch. Ground-based calibrations were not performed in such cold conditions, and cannot be used to derive this correction.

Values used for temperature correction are therefore determined using observations of the internal lamp during the in-flight calibration sessions. We thus got for each channel a set of intensity measurements of the calibration source at various temperatures, *i.e.* the output signal as a function of detector temperature. These 128 functions were fitted by second order polynomials to interpolate the values within the actual temperature range encountered during acquisition (typically -70° to -78° C). These variations of detectivity with focal plane temperature are used to bring back the measurements to -75 °C, the magnitude of the correction being ±4% (file SOURVOL.DET). This correction uses the value of temperature refreshed every 14 s. Variations of the transfer function with temperature are assumed independent of analogic gain (*i.e.*, gains are assumed independent of detector temperature).

Two problems remain at this step. First, the on-board calibration source was a simple filament, which filled only a small part of the field of view and lost its shape when heated, so the observations of the calibration lamp may not be comparable from session to session. We used the first spectrum of each series only, when the lamp was still cold in its rest position, which is assumed constant for the various calibrations sessions. Second, the levels of intensities of the lamp were incorrectly estimated, and most channels in the long wavelengths odd-row were saturated even at the lowest intensity of the lamp. Therefore these channels cannot be corrected from the variations of detectivity with temperature. Considering the magnitude of the correction on even channels, this is a major limitation when trying to recover the intensities in the odd channels.

This correction is accurate enough for even channels in most image cubes: after February 27th (Daedalia image cube) the temperature ranges from -75.4 to -77.4° C during observation. However, the two high-resolution (Pavonis and Biblis) and the first medium-resolution (Arabia) sessions were acquired at significantly higher temperatures (up to -70.4° C) for which this correction is not optimized. We derived a second-level temperature correction for those three sessions only, taking advantage of multiple observations in the region of Pavonis Mons. This area has been observed on February 11th and March 14th, respectively at high and low detector temperature, under similar viewing conditions. A ratio of carefully selected spectra yielded a set of coefficients for the largest temperature difference (file COEF.DEC). For intermediate temperatures a linear interpolation of this correction gives satisfying results on the first image cubes, in the sense that it yields similar spectra for bright regions with similar morphologies, though the accuracy is certainly reduced. This second order correction is applied on fully corrected spectra. It should be applied also to the spinning session (February 22nd).

Matching the spectral ranges

The short and long wavelength detectors are globally shifted relative to the optical path, and so are the two rows of detectors in a given spectral range. For 3-axes stabilized sessions on Mars, this results in a shift of images acquired in short and long wavelength channels of about one pixel along the slit. The match between the two spectral ranges (or between even and odd channels) could be improved by taking the short and long wavelength channels in different spectra, as described in section “Detectors and viewing geometry”. Strictly speaking, this procedure should be applied at this step after temperature correction (time dependent) and before deconvolution of spectral orders (space dependent). This procedure is useful only when extracting spectra from very small areas in non-uniform regions; it is not implemented in the calibration programs because it is only approximate and results in important loss of data (5-15% of the pixels); the next step (correction of spectral orders overlaps) is optimized without this correction. An acceptable alternative is to skip spectral range registration at this level, and to perform it after complete calibration when extracting spectra, if needed.

Correction of orders overlaps

The problem is now to recover a spectrum knowing the output of the detectors (*i.e.*, using notation from section “Instrument principle”, to recover $I(\lambda)$ knowing S_{Ch}). The three spectral components superimposed are processed one by one.

The β-coefficients, which correspond to the first and second orders overlap, could be estimated from both ground-based calibrations and measurements of separated optical and electronic parts of the instrument; however optical transmission was measured only below 2.5 µm, so the latter values are not available for the entire spectral range. During ground calibrations the instrument looked at a relatively cold black body (≈390 K) filling its field of view. At such a temperature, the thermal contribution is significant only above ≈2.0 µm, and can be completely neglected in the short wavelength range, *i.e.* below 1.55 µm. The output signal from the short wavelength range was thus entirely due to overlapping grating orders. In this case, the formula from section “Optical characteristics” becomes:

- in the long wavelength range, $S_{Ch} = I(\lambda) \cdot \alpha_{Ch}$,

where Ch ranges from 65 to 128 and λ from 1.64 to 3.16 µm.

- in the short wavelength range, $S_{Ch} = I(2\lambda) \,.\, \beta_{Ch} = \frac{S_{Ch'}}{\alpha_{Ch'}} \,.\, \beta_{Ch}$,

where Ch ranges from 1 to 64 and λ from 0.76 to 1.51 µm,
Ch' corresponds to 2λ.

The light source is a black body with known temperature, so we can derive the values of $\frac{\beta_{Ch}}{\alpha_{Ch'}}$ for each channel.

A remaining problem with these estimates lies at the very beginning of the spectral range, because the flux near 1.6 µm was too small to determine confidently the coefficients in the first four channels. These values were afterwards refined by statistical analysis of the corrected spectra.

Comparison of these experimental values and semi-theoretical ones derived from measurements of separated parts of the instrument (where they are available; see Fig. 7a and 7b) shows important discrepancies. Tests pointed out that experimental values are more accurate than semi-theoretical ones, in the sense that the former make it possible to correct Martian data from "echoes" of the CO_2 absorption band at 2 µm in the short wavelength range, while a correction using the latter doesn't yield such good results.

The smaller accuracy of semi-theoretical values for β prevents from using similar estimates for γ, but measurements of these coefficients could not be performed with the available calibration sources (this would have required a light source completely filtered above 1.1 µm). The γ coefficients where eventually derived from the flight data together with a first estimate of the α coefficients, by using two spectral models for Mars and Phobos. This models first relied on early estimates of the transfer function, and were progressively refined as our understanding of the surfaces increased (see the end of this section).

Given a spectral model for Phobos reflectance $r_p(\lambda)$, the signal in the long wavelength range is:

$$S_{Ch} = Sun(\lambda) \,.\, r_p(\lambda) \,.\, \alpha_{Ch} \,,$$

and coefficients α_{Ch} for the last 64 channels are readily derived. Knowing these coefficients we compute β_{Ch} coefficients in the short wavelength range from the above black body observations (file BETA.SPE).

In the short wavelength range, we can therefore remove the first order component. The

remaining signal writes:

$$S_{Ch} = Sun(\lambda) \,.\, r_p(\lambda) \,.\, \alpha_{Ch} + Sun(2\lambda/3) \,.\, r_p(2\lambda/3) \,.\, \gamma_{Ch} \,,$$

This first equation allows to compute α_{Ch} where γ_{Ch} is null. Using another spectral model for a bright region of Mars provides a second equation to compute both coefficient sets in the domain where γ_{Ch} is not null, *i.e.* between 1.1 and 1.45 µm (files ALPH0.SPE and GAMM0.SPE). The ratio $r_M(2\lambda/3)/r_M(\lambda)$ is the largest possible on Mars while it is comparatively small on Phobos, due to the very red continuum of the satellite's spectra. The two spectral models used, for Mars and Phobos, are described at the end of this section.

Transfer function for Mars

The main scope of the above procedure is to derive transfer coefficients for first and third order contributions to the measured radiance in the short wavelength range. Uncertainties in the coefficients estimates may thus result in systematic absorption-like features. Careful examination of spectral variations as a function of spectral slope ($r_M(2\lambda/3)/r_M(\lambda)$ and $r_M(2\lambda)/r_M(\lambda)$) shows that, in general, possible artifacts related to orders overlap cannot be separated from random noise and hence are of the same order, *i.e.* most of the first and third order contributions in the short wavelength range is actually removed.

However, this examination demonstrates the poor accuracy of α coefficients estimates (ALPH0.SPE), and the existence of systematic features correlated to reflectance in the short wavelength range. We therefore "recalibrated" the spectra by using another couple of spectral models for bright and dark regions of Mars (see the description of these models at the end of this section).

- in the long wavelength range, $\quad r(\lambda) = \dfrac{r'(\lambda)}{g_{Ch}}$

(so only one spectral model, for dark regions, is needed)

- in the short wavelength range, $\quad r(\lambda) = \dfrac{r'(\lambda) - O_{Ch}}{g_{Ch}}$

(and both spectral models are used)

where $r(\lambda)$ is the reflectance at wavelength λ,
$r'(\lambda)$ is the reflectance estimated with ALPH0.SPE,
g_{Ch} and O_{Ch} are recalibration gains and offsets (files COF7.SPE and OFF7.SPE).

In this procedure, the gains g_{Ch} represent a correction to the estimated transfer function α, while the offsets O_{Ch} account for a small amount of light coming from outside the nominal field of view, for possible differences in the magnitude of atmospheric scattering during the telescopic observations that were used as reference spectra, and for possible remaining contributions from first and third grating orders. The computed offsets are null by hypothesis in the long wavelengths range, and represent up to 7% of the average signal from Mars in the short wavelength range. No spectral model is available for Mars above 2.6 µm; in this range the gains are set to a constant value to fit the ratio at 2.6 µm. In other words, the calibration above this wavelength relies on the spectral model for Phobos with a scaling coefficient.

A first attempt to recalibrate the data made use of both spectral models for Mars also at longer wavelengths. The resulting offsets were decreasing with wavelength to very small values above 1.7 µm, on the order of the accuracy of the model (≈1% of the signal at 2.0 µm). Although this method provides consistent spectra, it is not conceptually better than the coefficient-only method, and assumes *a priori* knowledge of both dark and bright regions spectra. It was eventually dropped to minimize the number of hypothesis and to make it possible to study small features from 2.2 to 2.5 µm in bright regions spectra. The final gains and offsets proved to be usable on all Mars medium and high resolution image cubes.

Transfer function for Phobos

For observations of Phobos the stray light is expected to be different, and so are the offsets. The first Phobos image cube (actually a 1-pixel track) is acquired with Mars in the background, so the signal is badly contaminated by Mars reflected sunlight and is not recalibrated. The main image cube on Phobos is acquired with the sky in the background, so the stray light should be negligible. We therefore assume null offsets, and apply a gain-only correction.

The correction to the transfer function is derived from the spectral model for dark Martian regions. “Recalibration” gains for Phobos are computed as the ratio of a “precalibrated” spectrum (with ALPH0.SPE) of the reference area in Syrtis Major to the corresponding calibrated spectrum (using COF7.SPE and OFF7.SPE). Those gains are applied to several test areas on Phobos; the resulting spectra are then smoothed independently in the four spectral rows and the gains refined accordingly (file COEF.PHO). Smoothing is intended to minimize the propagation of calibration uncertainties from Mars to Phobos, since the darkest areas on Mars are four times brighter than Phobos.

The resulting calibration is probably less accurate for Phobos than for Mars. A particular

problem arises in the more eastern part of the image on the short wavelength, odd channels: as mentioned previously the signal in the dark sky is unexpectedly large in the first lines acquired, which is probably due to an internal reflection related to the unusual viewing geometry (phase angle is ~30° in the rest position of the mirror); this contribution is also present in spectra of Phobos in this part of the image and for these channels. Even channels are also affected by this phenomenon in the eastern part of the image, but to a much lesser extend.

Division by the solar spectrum

All data are divided by a standard solar spectrum weighted by the Mars-Sun distance on the date of observation. The solar spectrum used to compute the transfer function (SPECSOL.THE) is showed on Fig. 17. Original data are taken from Thekaekara 1975 and convolved with ISM spectral response. This spectrum represents the solar spectral irradiance (W m^{-2} μm^{-1}) at one astronomical unit from the Sun, divided by a factor of π. It is thus the amount of light reflected by a Lambertian surface normal to the Sun's direction at 1 a.u. The result of this final calibration step is a radiance factor (dimensionless).

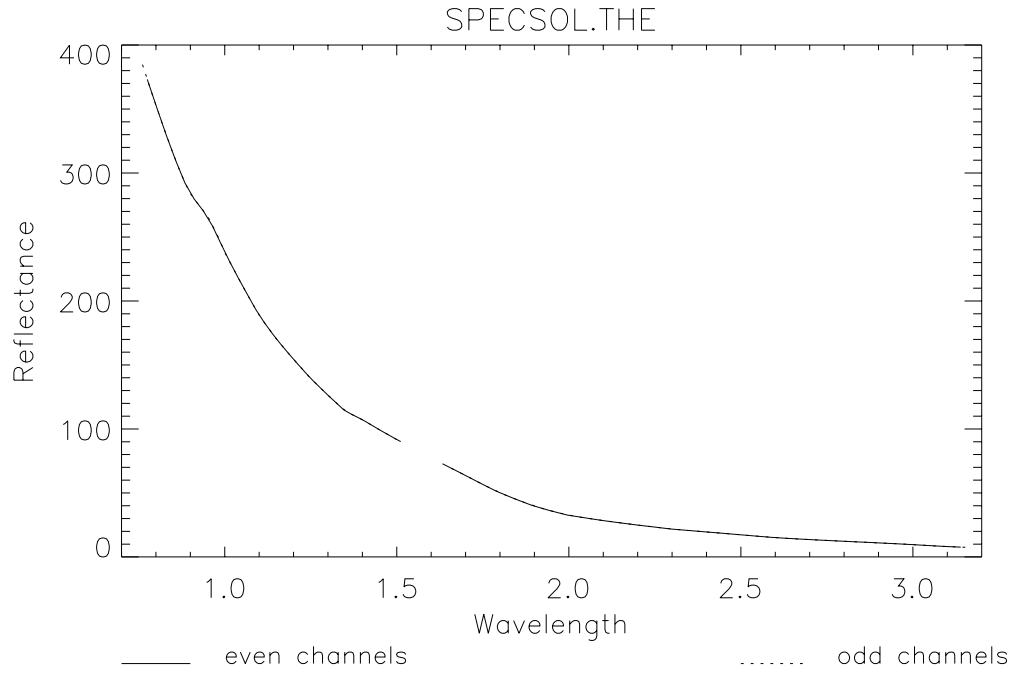

Figure 17: Solar spectrum used in the calibration process.

The solar spectrum was actually convolved with an early estimate of ISM spectral response and is not very accurate. However this spectrum was used to derive the transfer function, so systematic errors are compensated by the transfer coefficients, which must not be used with another solar spectrum. The correct manner to derive the radiance of the object within the field of view would be to compute its radiance factor following the above procedure, and then to multiply it by a properly scaled solar spectrum. Such a spectrum was computed by applying LECSPE.FOR to the original data from Thekaekara (file SPECSOL.NEW). It is similar to SPECSOL.THE but is integrated with the correct ISM response.

Results of the above calibration steps are stored in files with extension ".CAL", separately for odd and even channels. At this point, calibrated ISM spectra are sets of radiance factors measured at the corresponding wavelengths. Ratios of intensities in various channels are meaningful as well as ratios of different spectra, including spectra from different image cubes, but this information is not necessarily related to the surface itself. The most obvious features on Mars are actually due to atmospheric absorption; atmospheric scattering and photometric effects related to both the surface and the atmosphere also have a major incidence on the signal. Two optional calibration steps are included in the programs to address these problems on the first order. They are crude approximations of complex physical effects, that must be used with caution and may be improved.

Atmospheric absorption correction

Only sophisticated atmospheric models requiring large computer times make it possible to simulate properly the atmospheric absorptions. However a rough correction is included in the calibration programs to correct most atmospheric absorptions. This processing is optionally applied in ETALONNE.FOR; the resulting data files have the same format as calibrated data files and extension ".ATM".

This correction uses an absorption spectrum computed from ISM observations, and a simple atmospheric model. The atmospheric spectrum (LOGATM.SPE, see Fig. 18) is computed along the flank of Olympus Mons, and represents the absorption of a unit layer in the Martian atmosphere. In this region the surface can be considered homogeneous, while the depth of atmospheric features varies with altitude. The spectrum is computed from several ratios of normalized spectra at different elevations, then smoothed outside the atmospheric absorption bands (those are identified on a synthetic absorption spectrum representing a standard Martian atmosphere, computed with a library of spectral lines). The model assumes that the logarithm of atmospheric absorption varies linearly with the integrated airmass, *i.e.* with the column density. The ratio of logarithms of two band depths is therefore equal to the ratio of the respective cross-sections, which is independent of elevation. This would be a good

approximation if the atmospheric bands were spectrally resolved and unsaturated. In fact, the observed features result from the integration at ISM spectral resolution of many narrow lines, most of which are saturated; therefore absorption bands in ISM do not vary linearly with column density, and widen slightly with increasing airmass. Another problem is the possible lateral variation of mixing ratios of minor species; last, this method does not account for scattering by airborne particles.

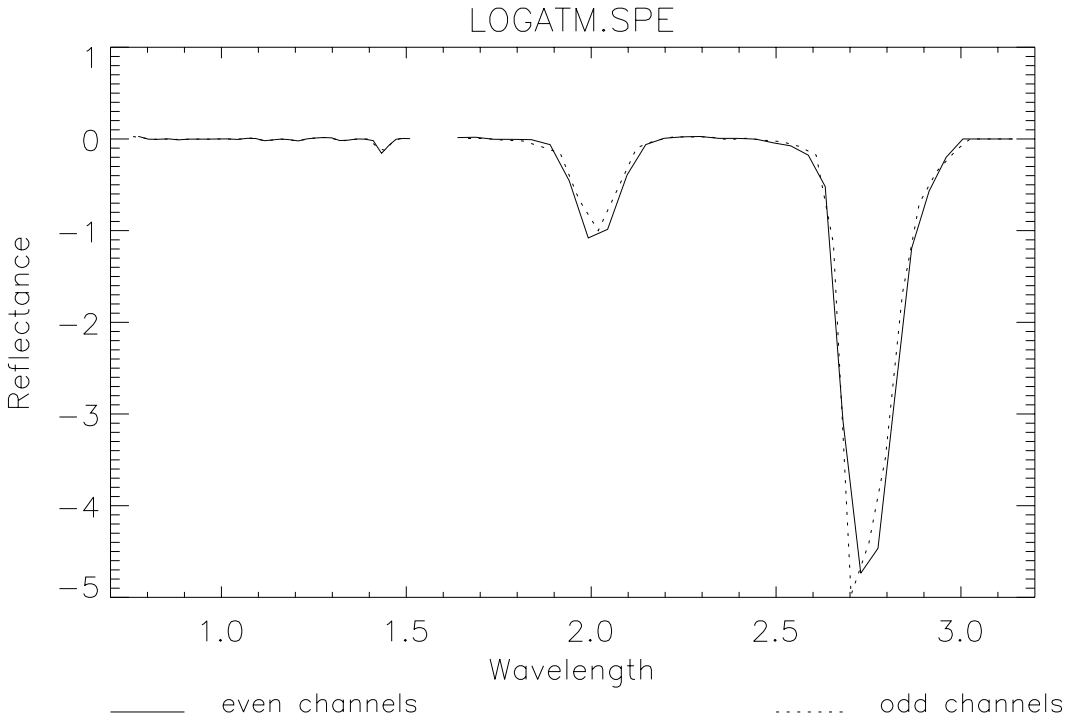

Figure 18: Spectrum used to compensate Martian atmospheric absorptions

As a consequence, this method can be used only to clean up the spectra, and does not work very well outside a given range of altitude. This is specially true for the nearly saturated CO_2 band at 2.7 µm. In particular, the correction does not allow detailed study of mineralogical absorption features overlapping the atmospheric bands, notably the bound-water bands between 1.85 and 2.1 µm.

Photometric correction

The overall reduction procedure yields a radiance factor of the observed body at each wavelength. On Phobos, the reflectance depends not only on the composition but also on the optical properties of the material; the amount of reflected light varies with incidence i, emergence e and phase angle ϕ, and is related to the texture of the surface. On Mars, the measured light is partly reflected by the surface but is also scattered and absorbed in the atmosphere, so the photometric dependence of the reflectance is more complicated. After compensating the gaseous absorptions atmospheric effects are still present in the spectra, mainly through aerosols scattering. Determination and correction of these effects is part of the scientific processing of the data and thus will not be handled here. However, a first order correction for photometric effects on Mars is provided in the mapping program PIXTRACE.FOR: when a map of intensity in a single channel is requested, limb darkening is optionally compensated by using the phenomenological Minnaert's model with a constant exponent at all wavelengths and albedos (see next section).

Uncertainty

The radiometric accuracy of the absolute calibration is limited by that of the reference spectra, by uncertainties in the solar flux, by changes in viewing geometry and by atmospheric variability of Mars. The absolute level of reflectance in a given channel is thus typically known within 15%-20%. For instance, the 1978 reference spectra (McCord *et al.* 1978) are scaled to "approximate normal reflectance", apparently by forcing the measurements in the visible to match previous data of 1969, more accurate in a photometric sense (McCord and Westphal 1971). However, the most recent (1986) photometric observations of Mars (Roush *et al.* 1992) are about 10% brighter in the infrared than the McCord *et al*. spectra; this discrepancy was ascribed to differences in illumination and viewing geometry. Such a systematic error in the absolute value of the reference spectra would however only result in a scaling coefficient for the albedo measured by ISM, and would not affect compositional interpretation (assuming that the ratio of the bright and dark reference spectra is comparable to that of the ISM spectra which were used in the calibration procedure).

The channel to channel accuracy (ratio of fluxes measured at different wavelengths) also depends mainly on the shape of the reference spectra, and on the accuracy of grating orders removal. After this correction about 3% of the remaining signal are due to the contribution of overlapping orders. There are three domains in the spectral range where removal of grating orders contributions may be significantly less accurate (by a factor of two): the first two

channels below 0.78 µm (where the first order contribution was difficult to measure), three channels between 1.07 and 1.14 µm (where the third order contribution may be different from zero, but impossible to correct since it comes from wavelengths below the lower limit of the instrument) and the first two channels of the long wavelength range between 1.63 and 1.70 µm (where no correction is applied while photons scattered in the second order might contribute to the measured intensity).

We verified that the calibration process doesn't introduce further uncertainty in the shape of the calibrated ISM spectra. First, the apparent absorptions are not constant within the data set, and are not systematically correlated to albedo; no prominent inverted absorption is observed either. Second, calibrated ISM spectra of Mars were satisfactorily compared to telescopic spectra at the highest signal-to-noise ratio and spatial resolution (from McCord *et al.* 1982, Singer 1982, and Bell *et al.* 1990). Two critical tests were performed by comparison with independent data sets; first below 1 µm, in the range where the recalibration offsets are the largest, with telescopic observations of the 1988 opposition (see Mustard and Bell 1994 for details); second above 2.0 µm with observations by the IRS spectrometers on board Mariner 6 and 7 in 1969 (the only other space borne observations in this spectral range so far. See Erard and Calvin 1997). In both cases the comparisons proved to be excellent, and the calibration procedure adequate. Since other possible errors are smaller, in most of the spectral range the channel-to-channel accuracy of the ISM spectra is similar to that of the more accurate telescopic spectra, which is typically of 3 to 5%. This limit of 5% may be underestimated beyond 2.6 µm where no observational reference spectra were used.

The uncertainty discussed above limits the interpretation of an absorption feature in an absolute spectrum, but not the meaningfulness of its variations between spectra. In other terms it would affect the average value of a ratio, as computed on a whole image-cube, but not its spatial variations within the image-cube. Factors limiting the relative (spectrum to spectrum) accuracy include removal of first and third orders contribution in the short wavelength range, removal of atmospheric absorption features in the reference spectra, temperature corrections, instrumental noise and linearity.

Instrumental noise is discussed in section "Electronics and on-board signal processing". Linearity was checked to be better than 0.5% for almost all observations; the only exception is the Ascraeus image cube, acquired at gain 3, in which four even spectels show some departure from linearity in the brightest area (see the same section).

The uncertainty on the removal of atmospheric features in the spectra used for calibration also decreases the accuracy within the atmospheric bands (namely the large CO_2 band from 1.95 to 2.09 µm and from 2.68 to 2.96 µm). Between 1.70 and 1.85 µm and in two spectels around 1.40 µm, the accuracy also depends on the precise content of water-vapor in the

reference spectra.

Temperature corrections shouldn't reduce relative accuracy, except in two cases: first when the second-level temperature correction is largest (Arabia image-cube), second for odd channels in the long wavelengths range. These channels can actually be used, but only to study relative variations between spectra acquired at very similar temperatures (typically with ratioed spectra from a given session).

The pixel-to-pixel variability is thus generally limited by the instrumental noise, that represents 0.3% of the signal in most of the spectral range. Below 0.78 µm, from 1.07 to 1.26 µm and from 1.63 to 1.70 µm, variations lesser than 0.5% may be meaningless. Above 2.6 µm the limit of 3% is imposed by the noise. These estimates are valid assuming a negligible contribution coming from the secondary diffraction peaks of the grating (*i.e.* no significant contribution of flux at another wavelength). This relative accuracy gives the real limit on the compositional interpretation.

Spectral models used for calibration

Early attempts to derive α coefficients involved various procedures, including pre-flight observations of reference light sources, comparisons of ISM data of Mars with comparable telescopic observations, and comparisons of ISM observations of Phobos with possible meteorite analogs. In first approximation, the three approaches converged to yield a consistent set of factors in most of the spectral range, although each has its own limitations. The final calibration makes use of all these elements, and includes three steps: first we derived a first-order estimate of the α and γ coefficients; second we performed a linear recalibration of Martian spectra to refine the final transfer function α and minimize the effects of stray light; third, this transfer function is adapted to Phobos observations with no correction for stray light. As detailed above, the first step requires one spectral model for Phobos and one for bright Martian areas; the second step uses a spectral model for a dark region of Mars, and another spectral model for bright regions used only in the short wavelength range; the third step uses only the dark region model.

No independent observations of Mars cover the whole spectral range of ISM. Ground-based near-infrared observations of Mars always end at 2.5-2.6 µm, because of very efficient H_2O and CO_2 absorptions in the terrestrial atmosphere. The only space-borne spectra in the near-infrared were acquired by IRS on Mariner 6-7; however the spectral domain only starts at 1.8 µm, and the spectral calibration of IRS data was not available at this time.

We selected two standard areas in the observed regions: Amazonis Planitia (west of

Olympus Mons) and Syrtis Major (west of the central ridge in the image cube); a dozen of ISM spectra were averaged in these areas to match the spatial resolution of ground-based observations. The reference spectra are telescopic observations of the same areas acquired under good conditions during the 1978 opposition (from McCord *et al.* 1978). The telescopic spectra, already corrected from terrestrial atmospheric absorptions, were convolved with the response function of ISM using LECSPE.FOR. All ISM and telescopic spectra were subsequently corrected for Martian atmospheric absorptions, using the model described above. This correction minimizes discrepancies at the corresponding wavelengths, and introduces no significant artifact below 2.6 µm. Above 2.6 µm where no spectral observation of Mars was available, only the spectral model for Phobos is used to calibrate the data.

The spectral model for Phobos is primarily based on the assumption that the measured spectrum of a particular spot on Phobos consists of light reflected from a material comparable to the L6 ordinary chondrite Pervomaiski, with an additive thermal component. This thermal component corresponds to a subsolar surface temperature of 295 K that was derived from preliminary results of both ISM and the KRFM radiometer.

Pervomaiski was chosen from among the various meteorite analogs for Phobos for two reasons. First, the preliminary calibrations of ISM spectra demonstrated that the surface material of Phobos has a very shallow hydration band at 2.8 µm. The “classical” meteoritic analogs from Viking observations are carbonaceous chondrites, that are usually hydrated. However Viking observations (ranging up to 1.2 µm only) are also consistent with altered ordinary chondrites, that are usually very dry; apart from the 3.0 µm hydration band, the main difference in this spectral range between those possible analogs is the depth of the 1 µm-silicate band. Second, the variability of this latter parameter on Phobos was found to be large, and covers the whole range of possible analogs (4% variation in band depth), which favours the assumption that Phobos spectra with the deepest 1 µm feature are similar to those of black chondrites. A reference spectrum of Pervomaiski was measured with the Relab spectrometer at Brown University; the spectral model was then adjusted to match the reflectance level and spectral slope of Phobos, as previously estimated with the transfer function derived from ground-based calibrations.

Uncorrected instrumental effects

Several problems remain after this calibration procedure in files “*.CAL” and “*.ATM”, mainly:

• The variations of channels response with temperature is poorly known in the long wavelength odd row. These measurements are therefore affected by a very large uncertainty.

• No registration of spectral orders or odd/even channels is performed, to avoid important loss of data. The procedure described in the next section can be applied if this level of accuracy is desired.
• The removal of the first grating order in the short wavelength track is effective short of 1.25 µm only. At longer wavelength the transfer coefficients β are unknown and no correction is performed, but the actual contribution is small.
• An unknown contribution of the second grating order may affect the first channel in the long wavelength range (channel 65).
• An unknown stray light contribution may remain in the long wavelength range in Mars data. In the Phobos data no correction for stray light is performed at all. A glare related to stray light was identified in the Phobos image, but is not corrected.
• The transfer function is computed with different methods below and above 2.6 µm. Intensities measured above 2.6 µm are probably less accurate, and may suffer systematic errors (possible offset of 1-3% reflectance).
• Gain 3 coefficients may be underestimated at short wavelength, due to the computation method. This would result in a systematic error on the spectral slope for sessions acquired at gain 3 on Mars (Ascraeus session and some small files extracted from calibration sequences). Phobos data acquired at gain 3 are not affected by this possible systematic effect.
• Several channels are saturated or in non-linear regime in the brightest half of the Ascraeus session (see the list of channels affected in this section). Estimated intensities are interpolated from correlations with neighbouring channels for even channels only (file "ASCEVEN.CAL"). Uncorrected calibrated data are available in file "ASCEVEN.CA0".
• The atmospheric correction provided here (files "*.ATM") is not good quality, particularly in the 2.7 µm band, and is not adapted to quantitative analyses.
• Photometric effects are known to affect the data (spectral slope and bands depth) and are not modeled here.

Calibration procedure

A short technical description of the calibration steps is given in this section. For details about the various dark currents files, detector temperatures, etc… see section “Observation sessions”. For further information about specific data sessions, see the file SESSIONS.ASC.

Registration of spectral measures

Channel intensities are registrated by performing a spatial convolution of corresponding spectral images. This point is discussed in section “Detectors and viewing geometry”.

Dark current subtraction

The original signal from the instrument is O_{Ch}. The dark current corresponds to the quantity called DC_{Ch} in the section “On-board processing”.

A list of the names of the dark current files to be used for each session is given in the section “Observation sessions”. The intensity in these files is divided by 2 at the end of each device to compensate analogic amplification. The coefficient 2 is not the actual value, and must be corrected to the value given in Table 4 below.

Gain correction

Values that must be used are listed in Table 4; they correspond to the product ΓΓ’ in the section “On-board processing”. Different values must be used for the beginning (first forty-eight channels) and end (last sixteen channels) of the two ranges (see section “On-board processing” and Fig. 8). The channel-specific values for the gain 3 are listed in the file GAIN3.VO2 (Fig. 9), they must be applied together with the gain-1 coefficients to correct for the amplification at the end of the devices.

These two steps can be summarized as:

$$S_{Ch} = \frac{O_{Ch} - DC_{Ch}}{\Gamma\Gamma'}$$

Nominal gain	Beginning of ranges	End of ranges
1	1	1.990
2	1.989	3.960
3	Channel dependent, see Fig. 9.	

Table 4: Analogic gains

Detector temperature correction

The correction to apply is a division of the spectrum S_{Ch} by

$$b1_{Ch} + b2_{Ch} . T + b3_{Ch} . T^2 ,$$

where T is the focal plane temperature in Celsius degrees, and b1, b2, b3 are the coefficients of the polynomials describing detectivity as a function of temperature (one polynomial per channel, file SOURVOL.DET). The result of this correction is the previous S_{Ch} — in digits — brought back to a detector temperature of -75°C.

The two high-resolution image cubes and the Arabia image cube are acquired at high temperatures, outside the range of efficiency of this correction. They requires an additional correction which is performed after division by the solar spectrum: intensities are divided by

$$b4_{Ch} . (T-70°C)$$

where $b4_{Ch}$ are the coefficients given in file COEF.DEC. This correction should also be applied to the spinning session (February 22nd).

Matching the spectral ranges

A global shift of images from short and long wavelength channels could be applied to improve registration (see section “Detectors and viewing geometry”). This procedure makes sense only for medium and high resolution sessions on Mars in 3-axes stabilized mode. In first approximation, the spectra can be recovered by shifting the orders by one pixel along the slit:

$S_{Ch}(l,s) = S_{Ch}(l, s)$ in the short wavelength range

$= S_{Ch}(l+1, s-1)$ in the long wavelength range.

A better approximation is to convolve the long wavelength channels images before registration:

$S_{Ch}(l,s) = S_{Ch}(l, s)$ in the short wavelength range

$= (1 - a) . S_{Ch}(l, s) + a . S_{Ch}(l+1, s-1)$ in the long wavelength range.

where a ranges from 0.5 to 0.9, depending on the spacing between lines of samples (*i. e.*, a varies slightly from session to session and within one session). Geographic coordinates computed by COORD.FOR correspond to spectrum (l,s). A similar registration of even and odd channels can be performed using a 2 pixels shift (see Table 2).

This correction is not performed in the programs, because it is not very accurate and results in loss of data (first sample and last line of the session); in addition, spectral orders deconvolution is not optimized with such a registration of spectral ranges. In the few cases where this correction is needed, it can be performed independently on fully calibrated spectra.

Removal of spectral order overlaps

Removal of first and third order contributions in the short wavelength range are performed in sequence. The long wavelengths part of the spectra is estimated by dividing S_{Ch} by the α-coefficients for the corresponding channels, which gives the irradiance from 1.64 to 3.16 µm (reflectance × solar spectrum). These intensities are weighted by the β-coefficients and then subtracted from the measured radiance at half wavelength, which removes the first order contribution in the short wavelength range.

In a second step, the intensity at the beginning of the short wavelength range (from 0.76 to 1.1 µm) is estimated by dividing this result by the α coefficients, weighted by the corresponding γ and subtracted from the signal between 1.15 and 1.53 µm (channels 31 to 64) where the third order contribution is not null. Each measurement is then an estimate — in arbitrary units — of the radiance at the corresponding wavelength.

The correction writes, for the short wavelength range only, with λ corresponding to Ch:

- In the first step (first order removal):

$$Sp(\lambda) = S_{Ch}(\lambda) - \beta_{Ch} . \varpi ,$$

where $S_{Ch}(\lambda)$ is the result of previous corrections,

β_{Ch} coefficients are the transfer coefficients listed in the file BETA.SPE,

$Sp(\lambda)$ is the result after this step, with $Sp(\lambda) = S_{Ch}(\lambda)$ in the long wavelength range where no spectral overlap occurs,

ϖ is the estimated radiance at double wavelength,

$$\varpi = \left\{ \frac{(2\lambda - \Lambda_1).S_{Ch}(\Lambda_2)}{\alpha(\Lambda_2)} + \frac{(\Lambda_2 - 2\lambda).S_{Ch}(\Lambda_1)}{\alpha(\Lambda_1)} \right\} . \frac{1}{\Lambda_2 - \Lambda_1} \quad ,$$

letting Λ_1 and Λ_2 be the ISM center wavelengths bracketing 2λ ($\Lambda_1 \leq 2\lambda \leq \Lambda_2$) for channels of same parity as Ch.

- In the second step (third order removal):

$$Sp'(\lambda) = Sp(\lambda) - \gamma_{Ch} . \varpi \ ,$$

where $Sp(\lambda)$ is the result of previous corrections (including first order removal),

γ_{Ch} coefficients are the transfer coefficients listed in the file GAMM0.SPE,

$Sp'(\lambda)$ is the result of this step, with $Sp'(\lambda) = Sp(\lambda)$ below 1.15 µm (channel 31) where the third order is filtered,

ϖ' is the estimated radiance at wavelength $\lambda' = 2\lambda/3$,

$$\varpi' = \left\{ \frac{(2\lambda/3 - \Lambda_3).Sp(\Lambda_4)}{\alpha(\Lambda_4)} + \frac{(\Lambda_4 - 2\lambda/3).Sp(\Lambda_3)}{\alpha(\Lambda_3)} \right\} . \frac{1}{\Lambda_4 - \Lambda_3} \quad ,$$

letting Λ_3 and Λ_4 be the ISM wavelengths bracketing $2\lambda/3$ ($\Lambda_3 \leq 2\lambda/3 \leq \Lambda_4$) for the channels of same parity as Ch.

<u>Conversion to physical units</u>

A first estimate of the radiance is obtained by a simple division:

$$I(\lambda) = \frac{Sp'(\lambda)}{\alpha_{Ch}} \quad ,$$

where $\lambda \in$ [0.76 ; 3.14 µm] and Ch $\in$ [1 ; 128] (*i.e.* for the whole spectrum),

α_{Ch} coefficients are listed in the file ALPH0.SPE.

Division by the solar spectrum

This correction must be performed with the solar spectrum used to compute the transfer function α. It writes:

$$R(\lambda) = I(\lambda) \cdot \frac{dist^2}{Sol(\lambda)} \quad ,$$

where dist is the Sun-Mars distance on the day of observation, in astronomical units,
$Sol(\lambda)$ is the solar spectrum at 1 a. u., resampled at ISM wavelengths and divided by π (file SPECSOL.THE),
$R(\lambda)$ is the "precalibrated" radiance factor.

The second level temperature correction is applied after this step for sessions acquired at high detector temperatures (Pavonis, Biblis, Arabia, and the spinning session).

Final calibration

The calibration of the data relative to previous ground-based observations of Mars is a simple linear transformation. This step is different for Mars and Phobos, because the stray light contribution is different.

$$r(\lambda) = \frac{R(\lambda) - o(\lambda)}{g(\lambda)} \quad ,$$

where $R(\lambda)$ is the "precalibrated" radiance factor,
$g(\lambda)$ and $o(\lambda)$ are the recalibration gains and offsets (files COF7.SPE and OFF7.SPE for Mars, or file COEF.PHO alone for Phobos)
$r(\lambda)$ is the calibrated reflectance of the planet (radiance factor).

For each session, odd and even channels measurements processed at this level are stored separately in files with extension ".CAL".

Correction of saturated channels in the Ascraeus image cube

Some channels are saturated (or non-linear) in the western part of the Ascraeus session. Reflectance values are estimated from correlations between these channels and neighbouring

ones as computed in the part of the session where no saturation occurs (for even channels only). Calibrated data (output of ETALONNE.FOR) are stored in ASCEVEN.CA0, corrected values are stored in ASCEVEN.CAL (processed by CORASC.FOR).

Atmospheric correction

The following correction can be applied to correct the largest atmospheric features in Martian spectra. This method works correctly only at relatively high surface elevations, and is often unsatisfying in the 2.7 µm band.

$$r_{surf}(\lambda) = \frac{r(\lambda)}{e^{atm(\lambda).a}} \quad ,$$

where $R(\lambda)$ as defined above,
$atm(\lambda)$ is the atmospheric spectrum measured from the data (which is already a logarithm, in file LOGATM.SPE),
R_{surf} is the spectrum corrected from atmospheric absorptions,
a is the depth of the 2 µm-CO_2 band defined as follows:

in even channels, $$a_e = Log\left\{\frac{R(73) + R(87)}{R(79) + R(81)}\right\} \quad ,$$

in odd channels, $$a_o = Log\left\{\frac{R(72) + R(88)}{2\ R(80)}\right\} \quad ,$$

where the argument of R is here for convenience the channel number.

For each session, odd and even channels measurements processed at this level are stored separately in files with extension ".ATM".

Photometric correction

The common way to correct the reflectance from major geometric effects is to divide it by the cosine of incidence. This corresponds to a Lambertian behavior, which is a theoretical limiting case approximated only by very bright and smooth surfaces. The situation is further complicated by aerosols scattering in the Martian atmosphere. Scientific study of the photometric variations showed that the Minnaert model can be applied with success on all

Martian sessions. On Mars, normal albedo can be estimated by dividing the radiance factors by:

$$\frac{(\cos i)^k}{(\cos e)^{k-1}} \qquad \text{where } k = 0.7$$

This procedure would bring all measurements back to a common viewing geometry (i = 0° and e = 0°). The Minnaert exponent of 0.7 is a compromise for various wavelengths, terrains, phase angles, and atmospheric conditions. It can lead to important errors at large incidence and emergence angles.

Concerning Phobos, the best approach is to use the Lommel-Seeliger model, or a Minnaert model with $k \approx 0.5$, with the actual viewing angles (taking local slopes into account). However, the actual photometric behavior is also strongly dependent on surface roughness, and varies slightly with the phase angle (not precisely known).

These photometric corrections are not applied to the files stored in the data base. The Minnaert model is used by PIXTRACE.FOR (Mars only) when plotting maps of intensity measured in a single channel to compensate limb darkening effects.

Orbits and observation modes

The nominal mission consisted in several phases: voyage to Mars; elliptic orbits around Mars, with high then low apocenter; circular orbits at the distance of Phobos; Phobos quasi-synchronous orbits; Phobos flyby; circular orbits again. The spacecraft was lost just before Phobos flyby. A detailed discussion of the mission schedule can be found in Sagdeev and Zakharov, 1989. During normal operations the spacecraft was three-axis stabilized, and ISM looked opposite the Sun when the mirror was in its rest position. In several occurrences however, stabilization was not maintain; in these cases the spacecraft spun around its principal axis of inertia, and the “anti-solar” axis of ISM described around it circles of unknown radius at an unknown speed. During observations of Phobos, the attitude of the spacecraft was modified to keep the “anti-solar” axis constantly pointed at Phobos. Data were transmitted on the night side of the orbits, so only one session was possible during each orbit (every eight hours during circular orbits), depending on the activity of other instruments.

A variety of observation modes was programmed in the instrument to optimize observations of Mars and Phobos from various types of orbits. Only three scientific modes were actually used in Martian orbit, the main characteristics of which are listed in Table 5. A calibration mode is also used before and usually after observations; last, a technical mode was used during cruise on two occurrences. All telemetry files are contained in the data base and described in FILES.ASC. Sessions containing usable information are decompressed by CONVERT.FOR and described in SESSIONS.ASC; they are calibrated by ETALONNE.FOR or ETALPHO.FOR whenever possible (two high resolution sessions on Mars from elliptic orbit; nine sessions on Mars from circular, stabilized orbit; main image cube on Phobos).

Instrument functioning is determined by an initialization sequence sent to the instrument. This sequence sets: starting observation time; length of observation (depending on memory allocation to ISM for this orbit); mode used (*i.e.* integration times and number of pixels per line); analogic gain; initial mirror position; gain and starting time for calibration sequences. Both starting time and initial mirror position determine the area observed.

Mode	Integration time	Pixels per line
Calibration sequence	1 s	1 (track)
Phobos flyby & default mode	1/8 and 1 s	1 (track)
Mars flyby # 1	1/8 s	8
Mars window # 0	0.5 s	25

Table 5: Observation modes used in flight

The Phobos flyby mode was used for the 1-pixel track on Phobos. It consists in sequences of two acquisitions with integration times of 0.125 s and 1 s, separated by 7.5 s. The mirror stays in its rest position, so there is only one pixel per line, looking in the "anti-solar" direction. The default mode used for the first two (uncalibrated) sessions from elliptic orbit is similar. The footprint for the Phobos track corresponds to a line of contiguous pixels near the Equator. For Mars, this mode was used only when the spacecraft was not stabilized but spun around its principal axis, so the pixels are not easily projected on the surface (focal plane temperature was also very high, so the data cannot be calibrated).

The Mars flyby mode was used for the two high resolution image cubes. Those were acquired from elliptic orbit, around the sub-solar meridian, near pericenter. Spectra are acquired consecutively, without rest between two acquisitions. From this altitude the integration time of 1/8 s yields spatially overlapping pixels, *i.e.* a continuous image, and pixel size is ≈5 km. In this mode and the following, a bug in the scanning program slowed the return of the mirror to its initial position at the top of the line. The instrument processor issued the same mirror command as long as the measured position of the mirror was not nominal. As a result, the instrument actually acquires 11 samples per line in this mode; the first three samples corresponds to the first mirror command, but are integrated while the mirror is returning to its more northern position: these measurements are correct, but spatial resolution is very poor. These first three samples must not be taken into account and are not extracted by CONVERT.FOR, which leaves eight samples per line.

The Mars window mode was used for the ten image cubes of Mars acquired from circular orbit, and for the Phobos image. The pixel size at the center of the disk is ≈20-25 km on Mars, ≈700 m on Phobos. One of the ten image cubes of Mars was acquired while the spacecraft was spinning and is not calibrated. Similarly to the Mars flyby mode, the first samples of the lines must be ignored: the instrument actually acquires 27 samples per line but the first two,

corresponding to the first mirror command, are acquired when the mirror is still moving. Twenty-five samples per lines are left which can be used. A similar mode with 50 sample per line (Mars global) is used for technical tests during cruise.

Calibration sequences consist in a series of observations of the sky and the internal source (see section “Encoding of special information”). They are always performed at 1 s integration time, with the mirror in rest position. All calibration sessions are decompressed by CONVERT.FOR, using a slightly different format. In particular mirror position is not refreshed in the telemetry blocks, so it is not written in the edited data files; calibration mode and gain are written instead.

Observation sessions

All telemetry files transmitted are included in the data base; description of the corresponding information is given in FILES.ASC. Eleven image cubes of Mars and one image cube of Phobos were acquired under satisfying conditions and are calibrated. Another image cube was acquired on Mars during a "spinning orbit", when the spacecraft was not stabilized; the identification of the observed areas on the surface of Mars is difficult, but these data could be calibrated. A second observation of Phobos was performed, but the signal is contaminated by reflected Mars signal and is hardly recovered. Other observations include: 30 calibration sessions, 2 cruise tests, 9 observations at the limb of Mars and 6 of Phobos during calibration sequences and extra sessions (extra lines acquired after or before a main session). All sessions with significant signal are decompressed and included in the data base; information about these secondary sessions is available in SESSIONS.ASC.

The main information about the primary sessions is listed in Table 6. Times are given according to the spacecraft clock, and correspond to acquisition of scientific data only. The first two sessions (high resolution image cubes) were acquired in Mars flyby mode from elliptic orbit. The following nine sessions are medium resolution image cubes of Mars acquired from circular orbit. The next one is the Phobos image cube, acquired in Mars window mode. Parameters for the Phobos track and the "spinning" session on Mars are listed separately.

Table 7 contains the estimated orbital parameters for the above Martian sessions, as well as the estimated shifts of the images. Pericenter time is given in UT. Pixels coordinates are computed from orbital parameters and then compared with altimetry maps from Viking and Mariner 9; shifts Δ_{lat} and Δ_{long} are applied to the whole image in COORD.FOR to refine the match with previous measurements (see section "Detectors and viewing geometry").

The projection of one of the Martian windows (12th March, in eastern Valles Marineris/Auroræ Planum) on the surface does not fit very well the topography retrieved from Mariner 9 and Viking observations, and may not be very accurate. This can be related to a sudden change in the attitude of the spacecraft with respect to the planet during acquisition; however Mariner 9 and Viking data appear relatively uncertain in this area. Orbital parameters for the spinning session (February 22nd) are similar to those for Arabia (February 21st).

Date	Start time	End time	Dark current file	Gain	First mirror command	Focal plane temperature (°C)
08/02	11:05:21	11:12:08	fond0802.dat	1	12	-71.2
11/02	16:51:43	16:58:00	fond1102.dg2	2	233	-70.4
21/02	10:23:03	10:44:58	fond2102.dg2	2	228	-72.2
27/02	2:41:42	3:08:51	fond2702.dg2	2	26	-75.8
01/03	10:45:28	11:12:36	fond0103.dg2	2	222	-76.5
07/03	3:00:47	3:27:53	fond0703.dat	1	2	-77.0
12/03	3:23:42	3:50:47	fond1403.dg2	2	2	-76.2
13/03	11:55:25	12:15:54	fond1303.dg2	2	156	-77.2
14/03	11:50:24	12:17:25	fond1403.dg2	2	210	-77.4
21/03	12:20:36	12:47:38	fond2103.dg3	3	162	-77.0
26/03	15:03:59	15:30:52	fond2603.dg2	2	198	-77.2
25/03	16:11:51	16:17:15	fond2103.dg3	3	240	-76.7
22/02	2:28:03	2:55:07		2		-72.3
25/03	15:49:28	15:58:39	fond1403.dg2	2	0	-77.4

Table 6: Characteristics of main sessions

Orbital parameters are not given for the Phobos session, due to the particular geometry of observation. The spacecraft is caught up by Phobos on its orbit, with a relative velocity of ≈45 m/s. Mars, Phobos and the spacecraft are aligned in the middle of the transit; therefore, both the distance and phase angle vary very much during transit (Fig. 19). The 1-pixel track observes the external hemisphere of Phobos, with Mars in the background; off-axis Martian reflected light actually contributes to the signal measured, to an unknown but significant level. The Phobos-spacecraft distance varies from 193 to 197 km, the phase angle from 15° to 21°. The following image cube observes the northern external trailing hemisphere of Phobos, with the sky in the background. The distance varies from 217 to 226 km, the phase angle from 28° to 31.5° when the mirror is in its rest position; phase varies by ≈5° along each scan line. This geometry implies that scanning is performed from East to West. There are 600 valid spectra in

the image cube, about 25% of which are pointing at the sky or at the limb. Files PIXLOC.CTR, PHO_COOR.DAT and PHO_SCRN.DAT contain coordinates of the pixels and observation angles in the Phobos image cube (see section “Detectors and viewing geometry” and SESSIONS.ASC).

Date	Mean distance (km)	Eccentricity	Inclination (°)	W (°)	w (°)	Time & day of pericenter	Δlong	Δlat
08/02	44490.10	0.904559	1.0230	191.451	77.252	5:52:42 8/2	-3.6	0.15
11/02	44489.00	0.904796	0.8720	196.817	72.137	11:28:12 11/2	-0.6	0.5
21/02	9667.47	0.012806	1.2870	125.739	317.259	1:56:50 21/2	-0.4	0.5
27/02	9667.64	0.012767	1.2790	123.233	321.834	18:11:02 26/2	0.0	0.3
01/03	9667.60	0.012984	1.2780	121.967	326.534	2:20:55 1/3	0.0	1.3
07/03	9668.66	0.012986	1.2786	120.390	330.076	18:35:20 6/3	0.0	1.3
12/03	9678.80	0.002493	1.0051	86.377	130.265	21:42:25 11/3	-1.2	0.5
13/03	9677.70	0.003107	1.0500	93.017	122.726	5:46:30 13/3	0.0	1.0
14/03	9677.70	0.003107	1.0500	93.017	122.726	5:50:40 14/3	0.0	0.7
21/03	9675.00	0.003018	1.0590	88.647	116.354	6:02:25 21/3	0.0	0.9
26/03	9379.56	0.031805	1.0750	84.093	356.560	6:17:50 26/3	0.0	1.3

Table 7: Orbital parameters for Mars sessions

Finally, Table 8 contains the description of observation conditions. The names of the sessions are derived from remarkable features in the area, avoiding as much as possible names already affected to USGS quadrangles; the first three letters (here in capitals) are used in file names related to these sessions. The number of spectra given in Table 8 is the number of calibrated spectra (entries with non-zero data in files “*.CAL”); they includes only spectra for which both odd and even blocks are present, and not integrated along the line (*i. e.*, in window mode the first pixels of each line are discarded), and spectra that can be interpolated from neighbouring pixels (see section “Detectors and viewing geometry”). The window size is given in lines × samples, including all measurements; this is the number of records in the data file (see section “Observation mode”). The last three columns give the longitude of the subsolar meridian, the areocentric longitude of the Sun, and the solar distance in astronomical units at the time of observation.

Name	Date	Spectra	Window size	Estimated local time	Phase angle	Solar Meridian	L_S	Mars-Sun dist (au)
PAVonis	08/02	2365	296 × 8	10:15-12:30	2.8° - 4.2°	100°	350.5°	1.547
BIBlis	11/02	2189	274 × 8	13:00-14:50	2.7° - 4.1°	100°	352.0°	1.551
ARAbia	21/02	2432	98 × 25	8:50-12:40	0.5° - 5.2°	335°	2.0°	1.563
DAEdalia	27/02	3013	121 × 25	11:30-15:45	5.5°-10.1°	165°	4.5°	1.570
SYRtis-Isidis	01/03	3005	121 × 25	8:50-13:20	1.7° - 6.3	270°	5.9°	1.572
V. Marineris (VMC)	07/03	3008	121 × 25	10:10-14:10	0.9° - 5.5°	100°	8.3°	1.580
AURoræ	12/03	3007	121 × 25	11:30-15:10	0.9° - 5.5°	70°	11.2°	1.585
OLYmpus	13/03	2275	91 × 25	12:10-15:10	14.5° - 19°	165°	11.7°	1.586
GORdii	14/03	3000	120 × 25	11:30-16:10	4.0° - 8.6°	160°	12.2°	1.588
ASCræus	21/03	2999	120 × 25	10:20-14:50	13.3°-19.7°	115°	15.6°	1.596
HEBes	26/03	2983	120 × 25	9:45-13:40	6.2°-10.9°	110°	18.0°	1.601
PHObos	25/03	600	24 × 25	–	28°-31.5°	~160°	17.5°	1.599
Elysium (SPIN)	22/02	3025	121 × 25	–	–	~220°	2.5°	1.564
Phobos track (PhT)	25/03	298	298 × 1	–	15°-21°	~160°	17.5°	1.599

Table 8: Characteristics of the main sessions

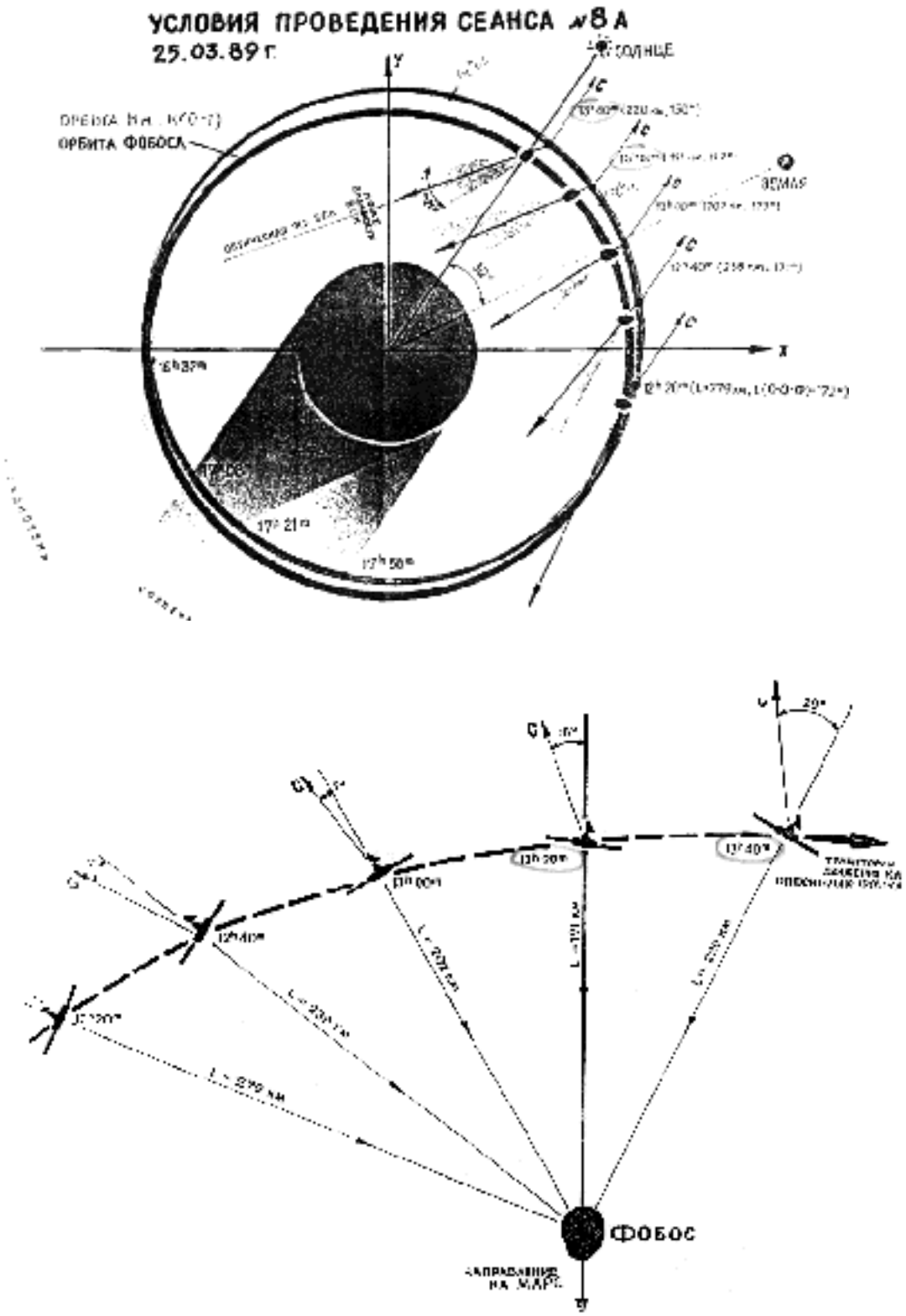

Figure 19: Geometry of the Phobos observations (25/03/1989). Times are given in Moscow time (= spacecraft time - 2h34'37"). Observations take place from 13h15 to 13h24 (track) and 13h38 to 13h44 (window).

Structure of data blocks

The ISM/KRFM complex supplies the spacecraft computer (Morion) with structured data blocks relative to both experiments. The spacecraft processor itself adds information to these data (spacecraft timing, checksum…) before transmission. Two ground stations received the data, checked their integrity and added information strings; data from both stations where thereafter compared, and a maximum number of consistent blocks were kept. These refreshed telemetry files are the ones included in the data base.

Data structure

The data files consist of blocks of 1 kbit each (128 8-bits characters) transmitted by the spacecraft. The first 960 bits are provided by the experiment, while the last 64 are added by the spacecraft processor (checksum, timing, etc…). Each data block from the spacecraft is followed by an information string of the same size written by the ETC (test and control device of the experiment) just after reception. These information strings contain information relative to the reception of the data only, and must be ignored for reduction purposes. The telemetry blocks themselves contain various type of information: ISM science or technical data, KRFM science or technical data. Only ISM science blocks are used here.

On Digital/VMS systems a “Vax block” contains 512 bytes, and thus corresponds to two data blocks with their information strings, *i.e*. to the space required to store one ISM spectrum. The Morion size is limited to 8 Mbits, so a maximum of 8192 data blocks is available during each session to store spectra, housekeeping information and calibration data.

Identification of block type. ISM science data

The first three bits of each block contain a code that identifies its type (technical, science ISM, science KRFM…). Only two types of blocks are used to reduce ISM data:

code 0 stands for ISM science-even block,

code 1 stands for ISM science-odd block.

Block parity (odd/even) refers to this identification code, not to channel numbers (see Table 9, Table 2 and Table 3). Each of these blocks contains measurements in 64 channels and main instrument parameters. A spectrum is thus always a couple of blocks, the even block being written first in the file, the odd one just after; they always contain the same timing information (hour, minute, second, eighth second), and must be identified according to this criterion.

	Channel sets
Odd blocks (1)	{ 1, 3, 5,…, 63 } and { 66, 68, …, 128 }
Even blocks (0)	{ 2, 4, 6 …, 64 } and { 65, 67 …, 127 }

Table 9: Channels written in science blocks

Reading and decompressing the blocks

The transmitted blocks are compacted. All parameters are stored on the minimum number of bits required: if a parameter can take five values it is written on three bits, etc… but strictly speaking, no compression is performed. The structure of the blocks must therefore be perfectly known to read them correctly.

The routine DDISM.FOR reads the data blocks and fills an array of 16-bits integers with the parameters. The most important ones are discussed in section “Encoding of special information”.

The values in the array returned by DDISM are not necessarily the actual values at time of acquisition: several parameters are not refreshed in each block, and the routine does not reset the array. For instance, the detector temperature is refreshed every 24 blocks, and the measured position of the mirror is written in the odd blocks only. The array will thus still contain the previous mirror position after reading an even block (the first block transmitted for a given spectrum) so this parameter cannot be used to check the correspondence between odd and even blocks (see section “Encoding of special information”).

One should also be aware that the various channels are not registered in sequence in the array. The order of the channels in the array returned by DDISM is also different between ground-based calibrations and flight data.

Encoding of special information

Reading the data files

Flight data files are read and decompressed by CONVERT.FOR. The files must be read as a succession of couples of blocks, each composed of 64 16-bits integers (or one 128-character string). The first block is the telemetry block, the second one is an information string added on ground, that contains no useful information. After reading the two blocks, the programs must call the routine DDISM to decompress the telemetry block and fill an integer array, hereafter called DATNUM.

Block type

The first element of this array identifies the block type. ISM science data blocks are identified by 0 and 1. Other types of blocks are useless for ISM reduction purposes. ISM technical blocks are only intended to monitor instrument functioning; all useful housekeeping parameters are contained in science blocks.

After reading an even block, the program waits for an odd block following immediately. Since one of the two blocks may have been lost during transmission, acquisition time must be checked to make sure that the two blocks correspond to the same spectrum.

DATNUM(1) = 0 means ISM science-even block
= 1 means ISM science-odd block

Time and date

All times registered in the data blocks are relative to the spacecraft clock. The time registered in the information strings refers to data reception on ground and must not be used. The difference between Morion time and Universal Time may have change during the flight due to resynchronizing of the spacecraft clock, but the difference remained constant while the spacecraft was orbiting Mars.

Morion time is given in DATNUM by:
Hour = DATNUM(8)
Minute = DATNUM(9)
Second = DATNUM(10)
Eighth-second = DATNUM(11) $\times$ 0.125

T. U. = Morion time - 20,077 s
= Morion time - 5.5769 h

Detector temperature

Several temperature measurements are made in various locations in the instrument and written every 24 science blocks. The temperature in Celsius measured in the focal plane (TDT1) is given by:

$T_{\circ C} = 49.96721 - 4.066708.10^{-2} \times TDT1$
where TDT1 = DATNUM(45)

Nominal gain

The two analogic gains are selected and stored independently. The overall gain is:
Gain = [Γ' + 1] $\times$ [2Γ + 1]
where Γ = DATNUM(16) and Γ' = DATNUM(17).

The result is the nominal value of the gain; the actual values are given in the section "Calibration procedure". Gain may vary between an observation session and the two associated calibration sessions; it may also vary during a calibration session. For this reason, it is written for each spectrum in the edited data files corresponding to calibration sessions.

Integration time

The integration time is determined by observing mode and remains constant during a session of observation, except in Phobos flyby mode, which alternates 1 s and 1/8 s observations (see section "Orbits and observation modes").

$$T_{int} = \frac{2^{integ}}{8} \quad ,$$

where integ = DATNUM(4).

Measured mirror angle

The measured position of the mirror, together with the attitude of the spacecraft, is used to compute the direction of observation and therefore the pixels projection on the surface. The angle in degrees with respect to the (anti-solar) rest position is:

$Ang_{deg} = (AGMR - 2048) \times 0.01308333$

where AGMR = DATNUM(65).

This parameter is written in the odd blocks only, so it cannot be used to identify two corresponding odd and even blocks.

Mirror command

This parameter is the order sent to the scanning device, according to the initialization sequence of the session. It is written in each science block, so it is used to check the presence of odd and even blocks corresponding to a single spectrum, and to identify missing spectra.

The code starts from a given position depending on the initialization sequence (see section “Observation sessions” for values). In the scanning modes used (Mars flyby and Mars window), this parameter is incremented by steps of +1 along a line, and then is reset to the initial value when the next line begins. Line and sample numbers are therefore easily recovered from mirror command, which is used to construct a consistent image cube. The first value of the mirror command appears twice in Mars window mode, and three time in Mars flyby mode; since the mirror is still moving during acquisition of these measurements, the corresponding samples are skipped in both modes (see section “Orbits and observation modes”).

This parameter is subject, as the rest of the block, to transmission errors, which can results in shifting problems when building the image cubes. Those errors are carefully corrected in CONVERT.FOR. Flight calibrations and observations in Phobos flyby mode are always performed with the mirror in its rest position (MIR_{Com} = 0 and AGMR = 2048). The parameter is not refreshed during calibrations, and the values read in the calibration blocks are meaningless; for this reason, mirror command is not written in edited data files for calibration sessions, but is replaced by gain and calibration step identifier.

MIR_{Com} = DATNUM(29)

Observation modes and calibration steps

A flag indicating whether the instrument is calibrating or observing can be checked.

DATNUM(5) = 1 during observation sessions,
= 0 during calibrations.

The specific observation mode is indicated by another code when this flag is on. The values used in orbits are:

DATNUM(6) = 0 Default mode (track).
DATNUM(6) = 1 Mars flyby (8 pixels per line)
DATNUM(6) = 2 Mars window (25 pixels per line)
DATNUM(6) = 3 Mars global (50 pixels per lines)
DATNUM(6) = 5 Phobos flyby (track).

One or several extra lines are sometimes acquired several minutes before (or after) a main session, and usually still have Mars in front of the instrument; those sessions are extracted and decompressed, but are not calibrated (see file SESSIONS.ASC). The times given in the section "Observation sessions" correspond to the beginning and end of the observation sessions and do not include in-flight calibrations or extra sessions.

In calibration mode (when DATNUM(5) = 0), DATNUM(6) indicates the current step in the calibration session. Eight successive steps are performed at 1 s integration time and programmable gain. Ten spectra are acquired in each step.

DATNUM(6) = 0 Dark sky
DATNUM(6) = 1 Obscurity (shutter closed)
DATNUM(6) = 2 Internal source, level 0 (off)
DATNUM(6) = 3 Internal source, level 1 (mini)
DATNUM(6) = 4 Internal source, level 2
DATNUM(6) = 5 Internal source, level 3 (maxi)
DATNUM(6) = 6 Same as 1
DATNUM(6) = 7 Same as 0

All calibration sessions are extracted and decompressed. Sky observations are occasionally performed with Mars or Phobos in the field of view, in which case they are extracted separately (see file SESSIONS.ASC).

References

Related documents contained in the data base include:

TECHNART.ASC (technical article about the instrument)
SESSIONS.ASC (description of observation sessions)
FILES.ASC (description of processed data files)
SOFTINFO.TXT (description of programs, routines and secondary products)

Publications related to analyses of ISM data are listed in the file PUBLISISM.ASC.

Bell, J.F., T.B. McCord and P.D. Owensby 1990. Observational evidence of crystalline iron oxides on Mars. *J. Geophys. Res.* **95**, 14447-14462.

Erard, S. and W. Calvin 1997. New composite spectra of Mars, 0.4-5.7 µm. *Icarus Icarus*, **130**, 449-460.

McCord, T.B., R.N. Clark and R.L. Huguenin 1978. Mars: Near-infrared spectral reflectance and compositional implications. *J. Geophys. Res.* **83**, 5433-5441.

McCord, T.B., R.N. Clark and R.B. Singer 1982. Mars: Near-infrared spectral reflectance of surface regions and compositional implications. *J. Geophys. Res.* **87**, 3021-3032.

McCord, T.B. and J.A. Westphal 1971. Mars: Narrow-band photometry, from 0.3 to 2.5 microns, of surface regions during the 1969 apparition. *Astrophys. J.* **168**, 141-153.

Mustard, J. and J. Bell 1994. New composite reflectance spectra of Mars from 0.4 to 3.14 µm. *Geophys. Res. Lett.* **21**, 353-356.

Roush, T., E. Roush, R. Singer and P. Lucey 1992. Estimates of absolute flux and radiance factor of localized regions of Mars in the (2-4 µm) wavelength region. *Icarus* **99**, 42-50.

Sagdeev, R.Z. and A.V. Zakharov 1989. Brief history of the Phobos mission. *Nature* **341**(6243), 581-618.

Singer, R.B. 1982. Spectral evidence for the mineralogy of high-albedo soils and dust on Mars. *J. Geophys. Res.* **87**, 10159-10168.

Thekaekara, M.P. 1975. The total and spectral solar irradiance and its possible variations. In *The Solar Constant and the Earth's Atmosphere* (H. Zirin and J. Walter, Eds.), pp. 232-251. Big Bear Solar Observatory, California.